https://doi.org/10.5194/egusphere-2026-6529
Preprint. Discussion started: 2 November 2026
© Author(s) 2026. CC BY 4.0 License.

# Spatial dynamics of volatile organic compounds (VOCs) in an urban environment and associated impacts on air quality

Finja Löher[1,2,a], Ines Bamberger[1,2], Markus Friedrich[1,2,3], Johann Schneider[3,2], Julian Bojanowski[3,b], Leyla Sungur[3,c], Manuel Steinbauer[4,2], Christoph Karl Thomas[3,2], Anke Christine Nölscher[1,2,d,e]

[1]Department of Atmospheric Chemistry, University of Bayreuth, 95447 Bayreuth, Germany
[2]Bayreuth Center of Ecology and Environmental Research (BayCEER), University of Bayreuth, 95447 Bayreuth, Germany
[3]Department of Micrometeorology, University of Bayreuth, 95447 Bayreuth, Germany
[4]Department of Sport Ecology, University of Bayreuth, 95447 Bayreuth, Germany
[a]now at: Wolfson Atmospheric Chemistry Laboratories, University of York, York, UK
[b]now at: Institute for Physics of the Atmosphere, Johannes Gutenberg-University, Mainz, Germany
[c]now at: Climate Service Center Germany (GERICS), Helmholtz Zentrum Hereon, Hamburg, Germany
[d]now at: Institute of Climate and Energy Systems, ICE-3: Troposphere, Forschungszentrum Jülich GmbH, Jülich, Germany
[e]now at: Institute of Geophysics and Meteorology, University of Cologne, Cologne, Germany

*Correspondence to:* Finja Löher (finja.loeher@york.ac.uk) and Anke C. Nölscher (a.noelscher@fz-juelich.de)

https://doi.org/10.5194/egusphere-2026-6529
Preprint. Discussion started: 2 November 2026
© Author(s) 2026. CC BY 4.0 License.



**Abstract**

Urban air pollution, affecting residents and commuters alike, depends considerably on volatile organic compounds (VOCs) due to their toxicity and potential to form secondary pollutants. The distribution and composition of urban VOCs reflect their emission as well as transport and atmospheric removal and formation processes. Hence, the VOC burden can differ substantially on small spatial scales. Aiming at investigating whether and how a large street canyon with dense traffic influences the air quality of adjacent neighbourhoods, we conducted trailer-based mobile measurements of nitrogen oxides, ozone, and VOCs in the city of Munich, Germany in September 2023. VOCs were measured using a highly resolved proton transfer reaction time-of-flight mass spectrometer (PTR-ToF-MS). To support different statistical analyses, the study area was divided into grid cells. A distinct separation of the VOC pool into traffic-related, biogenic, and functionalized compounds was achieved by hierarchical cluster analysis, ultimately assisting non-target analyses. The spatial variability was characterized by a combination of hierarchical cluster analysis, k-means analysis, and non-metric multidimensional scaling (NMDS). We show for exemplary locations that small-scale variations of some of the less abundant but highly reactive VOCs emitted by traffic (e.g. aromatics, alkenes) induce statistically significant spatial differences in terms of oxidant reactivities and the potential for the formation of aerosols or ozone. Finally, the variability-lifetime relationships of the VOC groups were analysed, revealing that the variability of the traffic-related VOCs was more tightly linked to local source strength compared to the biogenic and functionalized VOCs, and supporting their respective allocation.

https://doi.org/10.5194/egusphere-2026-6529
Preprint. Discussion started: 2 November 2026
© Author(s) 2026. CC BY 4.0 License.

## 1 Introduction

Air pollution is a major concern globally, causing millions of premature deaths each year according to the World Health Organisation (WHO). Residents of cities bear a disproportionate share of the burden, facing increased risks of respiratory and cardiovascular conditions (Gurjar et al., 2010; Hoek et al., 2013). While the troposphere has a considerable self-cleaning capacity, critical mixtures of volatile organic compounds (VOCs) and nitrogen oxides ($NO_x$=NO+$NO_2$) can increase the exposure to both primary and secondary pollutants and have therefore been the subject of research and policies. In case of VOCs, their impacts on air quality are manifold. Some VOCs are toxic and pose a direct risk to human and ecosystem health (Sweet and Vermette, 1992; Zhang et al., 2017). Furthermore, many VOCs are highly reactive and readily oxidized by hydroxyl radicals (OH), nitrate radicals ($NO_3$), or ozone ($O_3$). These reactions can alter ambient oxidant budgets and hence the capacity of the atmosphere to remove other pollutants (Lelieveld et al., 2008; Prinn, 2003). They can also promote the formation of secondary pollutants, including harmful ground-level $O_3$ (Haagen-Smit and Fox, 1954; Li et al., 2025) and secondary organic aerosol (SOA) adding to airborne particulate matter (PM) (Hallquist et al., 2009; Henze et al., 2008). The production efficiency of both SOA and $O_3$, in turn, are again strongly dependent on the ambient $NO_x$ concentration (Ng et al., 2007; Zhao et al., 2022). Apart from influencing the VOC oxidation mechanism and outcome, $NO_x$ species – especially $NO_2$ – are also severe respiratory irritants (Atkinson et al., 2018) and therefore pose a direct health risk in their own right as well.

With their high density of different activities, cities are affected by a broad range of pollutant sources. For nitrogen oxides, the largest source by far is road traffic due to the high-temperature combustion process (Beevers et al., 2012; Horowitz and Jacob, 1999). Urban sources of VOCs are more diverse and include heating, traffic and transportation, industrial processes, consumer products, cooking, and vegetation (Coggon et al., 2021; Do et al., 2014; Kumar et al., 2025; Martens et al., 2021; McDonald et al., 2018; Pfannerstill et al., 2024; Wang et al., 2023). Various VOC families have been highlighted in this context. Firstly, isoprene and terpenes are mainly emitted from trees and other vegetation mostly as a function of temperature, light, or environmental stress (Bai et al., 2015; Guenther et al., 1993). Pfannerstill et al. (2024) showed that biogenic terpenoids dominated the formation potential of secondary pollutants in the urban atmosphere of summertime Los Angeles. Secondly, compounds that were attributable to vehicular emissions – such as aromatic compounds – were long regarded as a major contributor to the VOC pool in cities but are recently discussed to become subordinate to VOC emissions from consumer and industrial products (Coggon et al., 2021; Do et al., 2014; Lewis, 2018; McDonald et al., 2018). Thirdly, oxygenated VOC such as methanol, acetone, and acetaldehyde were identified as the largest fraction of the urban VOC flux in the city of Innsbruck (Karl et al., 2018). Oxygenated compounds can enter the atmosphere as primary emissions but are mostly formed *in situ* from the oxidation of other hydrocarbons (Mellouki et al., 2015).

In order to ensure compliance with air quality standards, regulations have been put in place to reduce and control the ambient load of $NO_x$ and VOCs. Additionally, continuous measurements at stationary sites have been launched globally to provide a

https://doi.org/10.5194/egusphere-2026-6529
Preprint. Discussion started: 2 November 2026
© Author(s) 2026. CC BY 4.0 License.

record of the concentrations of critical species over long time periods. Such measurements are well-established for $NO_x$ as well as for $O_3$ and PM, with observations often spanning several years or even decades (Keuken et al., 2009; Lal et al., 2000; Masiol et al., 2019). More recently, stationary data of speciated VOCs have been recorded and used for profiling the urban VOC pool and for analysing its temporal variability, often in the context of seasonal changes and source appointments (Baudic et al., 2016; Jain et al., 2022; Kang et al., 2022; Li et al., 2022; Sheng et al., 2018; Valach et al., 2015; in 't Veld et al., 2024).

However, the representativeness of data from permanent measurement sites has been repeatedly questioned as any point measurement in cities is challenged by the heterogeneity resulting from mixing of the regional background with urban and street scale processes and emissions (Shi et al., 2016; Zhu et al., 2020). The interplay of local sources, city infrastructure, microclimate, synoptic conditions, airflow, atmospheric dynamics, and photochemical processes can cause substantial small-scale variations in urban air composition and quality which can only be fully described by observations that take place down to the same spatial resolution. With ongoing advances in technical and statistical tools, studies including mobile laboratories, sensor networks, and/or small-scale air quality models have become more feasible. Such studies demonstrated a substantial street-to-street variability of $NO_x$ and PM for instance in the cities of London (Wilde et al., 2024; Wilson et al., 2024), Munich (Zhu et al., 2020), Montreal (Wang et al., 2016a), or New York City (Jensen et al., 2009). Spatially continuous patterns of VOCs, on the other hand, are considerably more difficult to obtain. Given the need for more advanced instrumentation, extensive measurement networks quickly become impractical, and mobile campaigns remain technically and logistically challenging. In recent years, mobile urban VOC data have been recorded for instance from planes (Koss et al., 2017; Pfannerstill et al., 2023) or road vehicles (Liang et al., 2020; Rutherford et al., 2024; Wagner et al., 2021), yet information on the detailed spatial distribution of urban VOC is still extremely scarce.

This lack of data is a significant concern, as a detailed understanding of the occurrence and variability of VOCs is essential to better comprehend and ultimately mitigate urban air pollution, especially on street-level scales where local pollution events originate and develop. Here, we present the spatial and temporal variability of the mixing ratios of VOCs, $NO_x$, and $O_3$, as observed during a comprehensive mobile measurement campaign in an urban district in the city of Munich, Germany in September 2023. Given the emission from point sources such as traffic on the one hand, and the short lifetime of many compounds on the other hand, we expected high spatial and temporal heterogeneity. In particular, our study aimed at investigating whether and how a large street canyon with dense traffic would affect the air quality of adjacent neighbourhoods with residential and workplace functions.

https://doi.org/10.5194/egusphere-2026-6529
Preprint. Discussion started: 2 November 2026
© Author(s) 2026. CC BY 4.0 License.

## 2 Methods

### 2.1 Study area

The city of Munich has about 1.5 million inhabitants. Much of the city's traffic is channelled in the so-called Middle Ring, which is considered one of the most congested routes in Germany. In its north-western parts, the Middle Ring is almost perfectly aligned along a north-south axis named Landshuter Allee (Figure 1). With up to 8 lanes, the Landshuter Allee spans a width of around 54 m between the houses on either side of it. The airflows and atmospheric mixing in the street canyon are characterized in detail by Sungur et al. (2026). A tunnel of about 360 m length exists between the intersections of the Landshuter Allee with the Leonrodstraße and the Nymphenburger Straße respectively. Further south, the bridge Donnersberger Brücke leads over highly frequented train tracks. Lively mixed-use areas, residential and recreational areas, and industrial complexes line both sides of the Landshuter Allee (Figure S1, Supplement). Notably, roadside vegetation can be found along much of the length of the Landshuter Allee as well as in its western neighbourhood. The federal environmental agency (Bayerisches Landesamt für Umwelt; LFU) operates one air quality monitoring station on the Landshuter Allee and four other stations in the urban area of Munich (Stachus, Lothstraße, Johanneskirchen, Allach; Figure 1a).

### 2.2 Mobile laboratory

For the mobile measurements, a trailer was equipped with instrumentation for the analysis of the concentrations of various gas-phase species and for the acquisition of meteorological variables and turbulent airflow (Figure 2). On the roof of the trailer, the Inertial Navigation System (INS, for localisation and movement, at 50 Hz), an ultrasonic anemometer (for wind speed and direction and for sonic temperature, sampled at 20 Hz), and an open path infrared gas analyser (for carbon dioxide and water concentrations, also sampled at 20 Hz) were set up. The trailer interior was climatized to 30 °C and housed a proton transfer reaction time-of-flight mass spectrometer (PTR-ToF-MS) for VOC measurements as well as $O_3$ and $NO_x$ analyzers (Sect. 2.2.1 and 2.2.2).

The inlet for gas-phase measurements of VOCs, $NO_x$, and $O_3$ was installed on top of the trailer about 3.5 m above the ground and 50 cm above the roof of the trailer. The inlet was facing forward to avoid or minimise the risk of self-sampling (Wilde et al., 2024; Wilson et al., 2024). With this set-up, we aimed to sample air from in front of the moving vehicle, which was displaced upward and carried over the roof of the car and onto the top of the trailer. All data recorded while the car was not in motion (e.g. at intersections) were discarded for the statistical analyses to further minimize the risk of sampling the exhaust of the car towing the trailer.

The inlet system consisted entirely of insulated Teflon tubing. A 1/4'' line led into the trailer and passed through a particle filter before branching. The PTR-ToF-MS was connected with a 1/8'' line, while the NOx and $O_3$ analyzers were connected

https://doi.org/10.5194/egusphere-2026-6529
Preprint. Discussion started: 2 November 2026
© Author(s) 2026. CC BY 4.0 License.

with another 1/4'' line. The length from the inlet to each instrument was approximately 2 m. Based on calculations of the flow regime and confirmed by response tests, the inlet system residence time was less than one second. The $NO_2$ detector had a slower response time than the other instruments, which we quantified based on the cross correlation of $CO_2$ and $NO_2$ which were measured outside and inside the trailer, i.e. without and with passing through the inlet line, respectively. This calculation was based on the assumption that both compounds are emitted mainly from traffic and should therefore have congruent spatio-temporal patterns, with different sampling times being the main source of disparity. The determined temporal lag was 12 s (Figure S2, Supplement) and was corrected accordingly.

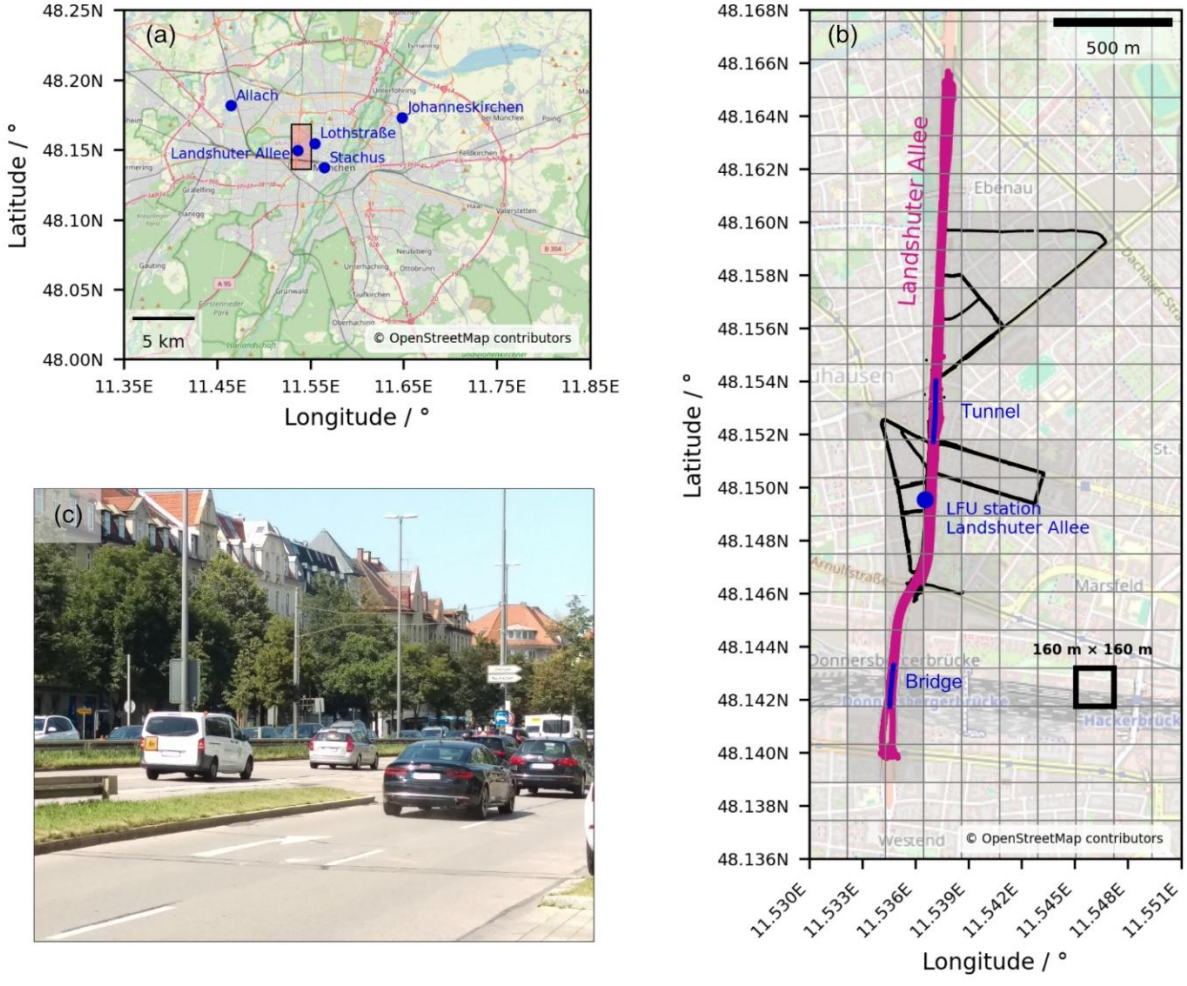



**Figure 1: Overview of the study area. (a) Map of the city of Munich. The coloured box shows the position of the study area within the city. LFU monitoring stations are depicted. (b) Study area around the Landshuter Allee in Munich, Germany. Route 1 followed the Landshuter Allee street canyon (shown in purple) while route 2 covered the neighbourhood (shown in black). The study area was separated into grid cells for the statistical analyses, with a grid cell size of 160×160 meters. (c) Photo of the Landshuter Allee close to the LFU monitoring station (taken in August 2020). Base maps from OpenStreetMap, distributed under the Open Data Commons Open Database License (ODbL) v1.0, https://www.openstreetmap.org/copyright.**

https://doi.org/10.5194/egusphere-2026-6529
Preprint. Discussion started: 2 November 2026
© Author(s) 2026. CC BY 4.0 License.

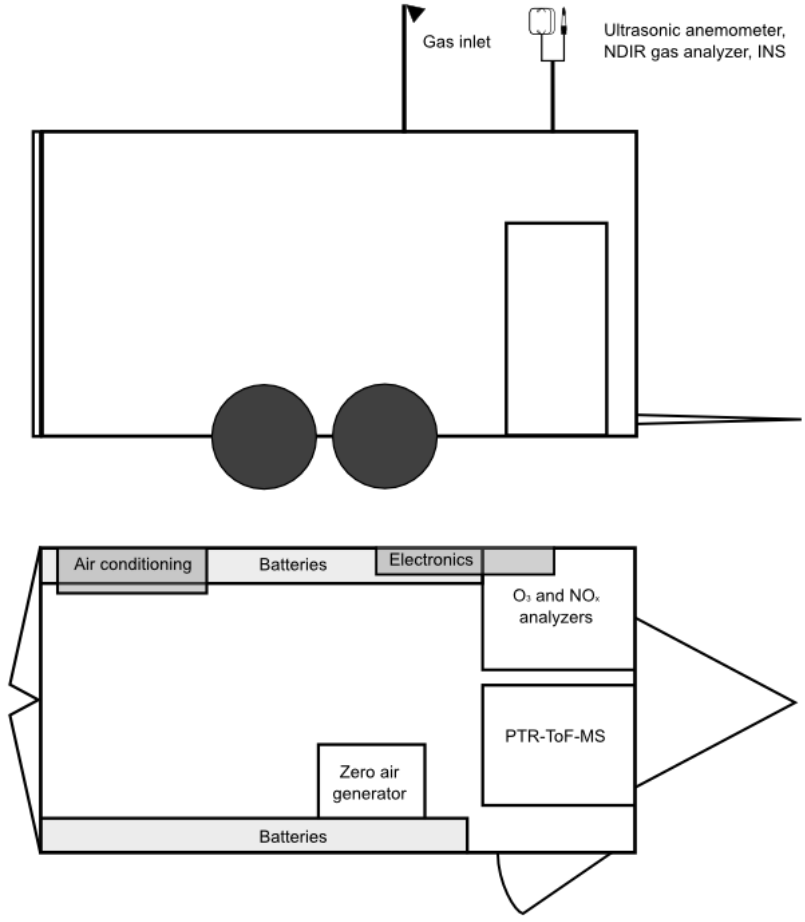



**Figure 2: Trailer (side view and top/internal view) equipped with instrumentation for mobile gas-phase measurements. NDIR gas analyzer = non-dispersive infrared gas analyzer; INS = inertial navigation system; PTR-ToF-MS = proton transfer reaction time-of-flight mass spectrometer.**

### 2.2.1 PTR-ToF-MS

The PTR-ToF-MS (IONICON, PTRTOF 4000) used for VOC measurements had a mass resolution of about 4000 m/Δm, allowing the differentiation of compounds with the same nominal mass (Graus et al., 2010; Romano and Hanna, 2018). We used hydronium ions ($H_3O^+$) as primary ions (PI) and measured all compounds at their protonated masses (Table 1) with a time-resolution of one second. Since PTR is a soft ionisation technique with low fragmentation, most compounds have a strong signal for the $[M+H]^+$ ion (Lindinger et al., 1998). The PTR-ToF-MS was operated with a drift tube pressure of 2.6 mbar and a reduced electric field strength of E/N = 95 Td to further minimize fragmentation. Coil springs were attached to the instrument to accommodate the operation within the trailer without damage.

https://doi.org/10.5194/egusphere-2026-6529
Preprint. Discussion started: 2 November 2026
© Author(s) 2026. CC BY 4.0 License.

We calibrated the PTR-ToF-MS using a standard gas mixture of 12 compounds (mixing ratios between 917 and 1002 ppbv in $N_2$) with 5 dilution levels in the range of 0 to 20 ppbv. We performed one calibration before and one after the measurement campaign. Both times, we calibrated the instrument for relative humidities of 0, 35, 60, and 95%. For each calibration and humidity, the calibration curve was based on the background-corrected and PI-normalised values and forced through the origin. The sensitivity for a given compound was averaged across calibrations and humidity levels (agreement within 20% for every compound).

Table 1 lists the exact species for which the PTR-ToF-MS was calibrated. We assign this speciation throughout this study in order to use compound-specific reactivities for the calculation of photochemical indicators, but acknowledge that PTR-ToF-MS offers no structural resolution and that interferences from isomers or fragmentation of larger compounds are possible, such as for isoprene (Coggon et al., 2024) or the monoterpenes (Tani et al., 2003). In addition to the quantitative analysis of these target species, we evaluated the entire mass spectrum and tentatively assigned compounds to prevalent masses, with specific attention on VOCs reported in similar urban studies (Table S1, Supplement). These compounds were evaluated qualitatively only.

**Table 1: List of species calibrated for the PTR-ToF-MS. The sensitivity and the associated uncertainty are derived from the average of several calibrations at different humidity levels and before and after the campaign.**

| Compound | Sum formula | [M] / g mol$^{-1}$ | $[M+H]^+$ / m/z | Selected peak / m/z | Sensitivity / ncps ppbv$^{-1}$ | Uncertainty |
|---|---|---|---|---|---|---|
| Methanol | $CH_4O$ | 32.04 | 33.0335 | 33.0321 | 19.95 | 0.196 |
| Acetonitrile | $C_2H_3N$ | 41.05 | 42.0338 | 42.0330 | 58.05 | 0.146 |
| Acetaldehyde | $C_2H_4O$ | 44.05 | 45.0335 | 45.0326 | 52.71 | 0.135 |
| Acetone | $C_3H_6O$ | 58.08 | 59.0491 | 59.0479 | 75.32 | 0.156 |
| Isoprene | $C_5H_8$ | 68.12 | 69.0699 | 69.0682 | 41.14 | 0.145 |
| Benzene | $C_6H_6$ | 78.11 | 79.0542 | 79.0529 | 54.03 | 0.175 |
| 2-Methyl-2-Pentene | $C_6H_{12}$ | 84.16 | 85.1012 | 85.0996 | 20.00 | 0.144 |
| Toluene | $C_7H_8$ | 92.14 | 93.0699 | 93.0690 | 71.28 | 0.169 |
| *m*-Xylene | $C_8H_{10}$ | 106.16 | 107.0855 | 107.0851 | 81.98 | 0.167 |
| 1,2,3-Trimethylbenzene | $C_9H_{12}$ | 120.19 | 121.1012 | 121.1003 | 72.35 | 0.163 |
| *m*-Diethylbenzene | $C_{10}H_{14}$ | 134.22 | 135.1168 | 135.1171 | 84.69 | 0.157 |
| $\alpha$-Pinene | $C_{10}H_{16}$ | 136.24 | 137.1325 | 137.1319 | 37.30 | 0.147 |

https://doi.org/10.5194/egusphere-2026-6529
Preprint. Discussion started: 2 November 2026
© Author(s) 2026. CC BY 4.0 License.

We used the Ionicon Data Analyzer (IDA, v2.1.1.2) for spectral analysis and peak integration. All other data processing was performed in Python (v3.9.7), including normalisation to the reagent ion, background subtraction, and quantification (if applicable). For the PI normalisation, we considered the signal of $H_3O^+$ at *m/z* 21.0220 as well as the water clusters $H_3O$-$H_2O^+$ and $H_3O$-$(H_2O)_2^+$ at *m/z* 39.0325 and *m/z* 55.0382 respectively.

#### 2.2.2 $O_3$ and $NO_x$ analyzers

To increase accuracy, we measured both NO and $NO_2$ directly. For $NO_2$ detection, we employed an instrument using cavity attenuated phase shift (CAPS) spectroscopy (Teledyne, T500U), whereas a chemiluminescence detector (CLD) was available for NO measurements (ECOPHYSICS, nCLD 855 AL2). $O_3$ was recorded by a UV-photometric $O_3$ analyzer (Thermo, 49i). Prior to the campaign, the instruments were calibrated using a dilution calibrator and gas-phase titration (Teledyne, T750U).

### 2.3 Mobile measurements

We performed mobile measurements in the vicinity of the Landshuter Allee between September 10$^{th}$ and September 18$^{th}$, 2023. The weather conditions in this time period displayed little day-to-day variability, with low wind speeds typically below 1.5 m s$^{-1}$, air temperatures mostly between 20 and 25 °C, and clear skies except for some rain on September 13$^{th}$ when no measurements were taken (Figure S3, Supplement). In total, we made 12 rides on 8 days, covering different days of the week and different times of the day (Table S2, Supplement). We defined two different routes which we followed repeatedly with minimal variations due to roadworks. Route 1 (R1) covered the Landshuter Allee street canyon and the tunnel, whereas route 2 (R2) focused on the neighbourhoods east and west of the Landshuter Allee (Figure 1b). The number of loops per ride varied according to the battery charge of the trailer and the traffic density but added up to 57 loops in total (30×R1, 27×R2). Throughout the rides, we obtained hourly background values for the VOCs, $NO_x$, and $O_3$ by measuring zero air for 5 minutes.

### 2.4 Statistical analysis

For investigating spatial patterns of gas-phase species, we separated the study area into distinct grid cells (Figure 1b). We selected a grid cell size of 160×160 m that was effective in detecting small-scale differences and clearly differentiating between the Landshuter Allee and minor adjacent streets while not being too computationally expensive and still retaining enough data per grid cell to derive meaningful interpretations. A single value for each of the measured compounds for each grid cell was compiled by averaging the recorded mixing ratios in that grid cell across all rides. For most of the analyses (specified in more detail in the following), the values of each individual species were normalized across all grid cells to avoid bias towards compounds with high mixing ratios. This was especially relevant for NO, $NO_2$, and $O_3$, which often exceeded some of the VOC mixing ratios by more than one order of magnitude.

https://doi.org/10.5194/egusphere-2026-6529
Preprint. Discussion started: 2 November 2026
© Author(s) 2026. CC BY 4.0 License.

In a first step, we aimed at providing a bulk analysis of the air composition in each grid cell by taking into account all gas-phase species (VOCs as well as NO, $NO_2$, and $O_3$). The normalized data of these species were analysed by hierarchical clustering, using Euclidean distance to quantify pairwise dissimilarities between grid cells and the Ward's method as linkage function. Four distinct spatial clusters of grid cells with a similar composition of gas-phase species were identified after applying a distance cut-off at 1.8. We then performed further complementary analyses to increase robustness as well as to focus on the influence of either the inorganic (NO, $NO_2$, and $O_3$) or organic (VOCs) species in the study area. To do so, the grid cells were classified according to their mixing ratios of $O_3$ and $NO_x$ (sum of NO and $NO_2$). K-means clustering was used to identify three clusters of grid cells. As k-means provides a measure of similarity in the space of the measured variables (here: $O_3$ and $NO_x$), we used the non-normalized data in order to better represent photochemical regimes. Finally, all measured and calibrated species (VOCs as well as NO, $NO_2$, and $O_3$) were analysed using non-metric multidimensional scaling (NMDS). NMDS is an ordination method where objects (here: grid cells) are placed within an ordination space with reduced dimensionality but preserved dis-/similarities (Legendre and Legendre, 1998). It allowed not only for an investigation of links between the grid cells but also of links between the mixing ratios of gas-phase species that defined the ordination space. Here, the NMDS was calculated based on the normalized dataset using Euclidean distance for a two-dimensional space. We ultimately used the NMDS results to classify grid cells based on their association with specific VOCs in the ordination space.

While the above analysis allowed for the identification of similar locations within the study area, we furthermore used hierarchical cluster analysis to group the individual VOCs by their spatial co-abundance. The procedure was the same as for the hierarchical cluster analysis described above, except for that we transposed the dataset and performed the analysis solely for the VOCs. A distance cut-off at 2.2 was applied to identify three main clusters.

### 2.5 Calculation of air quality metrices

Several metrices were calculated to constrain the impact of the ambient VOC load on air quality. Firstly, the sum loss rates (total reactivities) for each of the main atmospheric oxidants – OH radicals, $O_3$, and $NO_3$ radicals – were characterized by referring to the rate coefficients for their reactions with each of the VOCs (Eq. 1). Additionally, the SOA yield (SOAy) and the maximum incremental reactivity (MIR) of the VOCs were calculated to assess the potential to form SOA (Eq. 2) and $O_3$ (Eq. 3) respectively. The compound-specific rate coefficients, SOAy values, and MIR values were obtained from literature values as listed in Table S3 (Supplement).

$$k'_{ox} = \sum k'_{ox,VOC} \quad (1a)$$

$$k'_{ox,VOC} = k_{ox,VOC} \times C_{VOC} \quad (1b)$$

https://doi.org/10.5194/egusphere-2026-6529
Preprint. Discussion started: 2 November 2026
© Author(s) 2026. CC BY 4.0 License.

where $k'_{Ox}$ is the total loss rate of the oxidant due to all VOC reactions (in $s^{-1}$) $k'_{Ox,VOC}$ is the pseudo first order rate constants of the loss of the oxidant due to the reaction with a specific VOC (in $s^{-1}$), $k_{Ox,VOC}$ is the second order rate constant of the reaction between the oxidant and the VOC (in $molecules^{-1}$ $cm^3$ $s^{-1}$), and $C_{VOC}$ is the VOC number concentration (in molecules $cm^{-3}$).

$$SOAP = X_{VOC} \times SOAy \quad (2)$$

where SOAP is the SOA formation potential (in ppbv), $X_{VOC}$ is the VOC mixing ratio (in ppbv), and SOAy is the dimensionless SOA yield of a specific compound.

$$OFP = M_{VOC} \times MIR \quad (3)$$

where OFP is the $O_3$ formation potential (in µg $m^{-3}$), $M_{VOC}$ is the mass concentration (in µg $m^{-3}$), and [MIR] is the maximum incremental reactivity (in g $g^{-1}$) of a specific compound. For easier interpretability, we converted the $O_3$ formation potential to a mixing ratio (in ppbv) by taking into account the molar mass of $O_3$.

https://doi.org/10.5194/egusphere-2026-6529
Preprint. Discussion started: 2 November 2026
© Author(s) 2026. CC BY 4.0 License.

## 3 Results and discussion

### 3.1 Variation in mixing ratios of nitrogen oxides and ozone

The daytime spatial patterns for NO (Figure 3a), $NO_2$ (Figure 3b), and $O_3$ (Figure 3c) differed greatly from each other. The highest mixing ratios of NO and $NO_2$ were found in the Landshuter Allee street canyon. There, traffic is particularly dense and ventilation is restricted by the high and closely spaced surrounding buildings, the absence of open areas, and the passage of vehicles through the Landshuter Allee tunnel (Sungur et al., 2026). Furthermore, the areas arounds intersections were identified as hotspots, consistent with previous literature (Zhu et al., 2020). The mixing ratios of NO varied substantially up to around 200 ppbv, with extremes in the ppmv range, and an average (± standard deviation) of 26.5 ± 45.6 ppbv (median 11.3 ppbv) for the entire campaign period and study area. $NO_2$ mixing ratios peaked at 297 ppb but mostly remained below 75 ppbv. The $NO_2$ average was 22.7 ± 17.7 ppbv (median 18.4 ppbv). In contrast, $O_3$ showed a smaller spatial variability throughout the study area than the nitrogen oxides. The ambient $O_3$ mixing ratios were all < 42 ppbv, with an average of 12.1 ± 7.1 ppbv (median 10.0 ppbv).

At night, the spatial patterns were similar to those at daytime, but the mixing ratios for NO (Figure 4a), $NO_2$ (Figure 4b), and $O_3$ (Figure 4c) were generally lower with averages of 9.4 ± 22.6 ppbv (median 1.0 ppbv), 10.7 ± 4.7 ppbv (median 9.3 ppbv), and 4.8 ± 1.3 ppbv (median 4.8 ppbv), respectively. Hence, the average mixing ratios of $NO_x$ and $O_3$ were about a factor of 2 to 3 lower than during daytime, which is likely due to the absence of traffic as a main source of $NO_x$ and various VOCs on the one hand, and due to the absence of solar radiation which is needed for the production of $O_3$ on the other hand.

For comparison, the LFU monitoring station on the west side of Landshuter Allee recorded mixing ratios for NO and $NO_2$ of 25 ± 25 ppbv (median 17 ppbv) and 24 ± 12 ppbv (median 21 ppbv) during the measurement period (respective averages across both daytime and nighttime). For the same timeframe, $O_3$ mixing ratios in the city of Munich varied between 25 and 29 ppbv (averages at the four LFU monitoring stations Allach, Johanneskirchen, Stachus, Lothstraße; medians 22-26 ppbv).

https://doi.org/10.5194/egusphere-2026-6529
Preprint. Discussion started: 2 November 2026
© Author(s) 2026. CC BY 4.0 License.

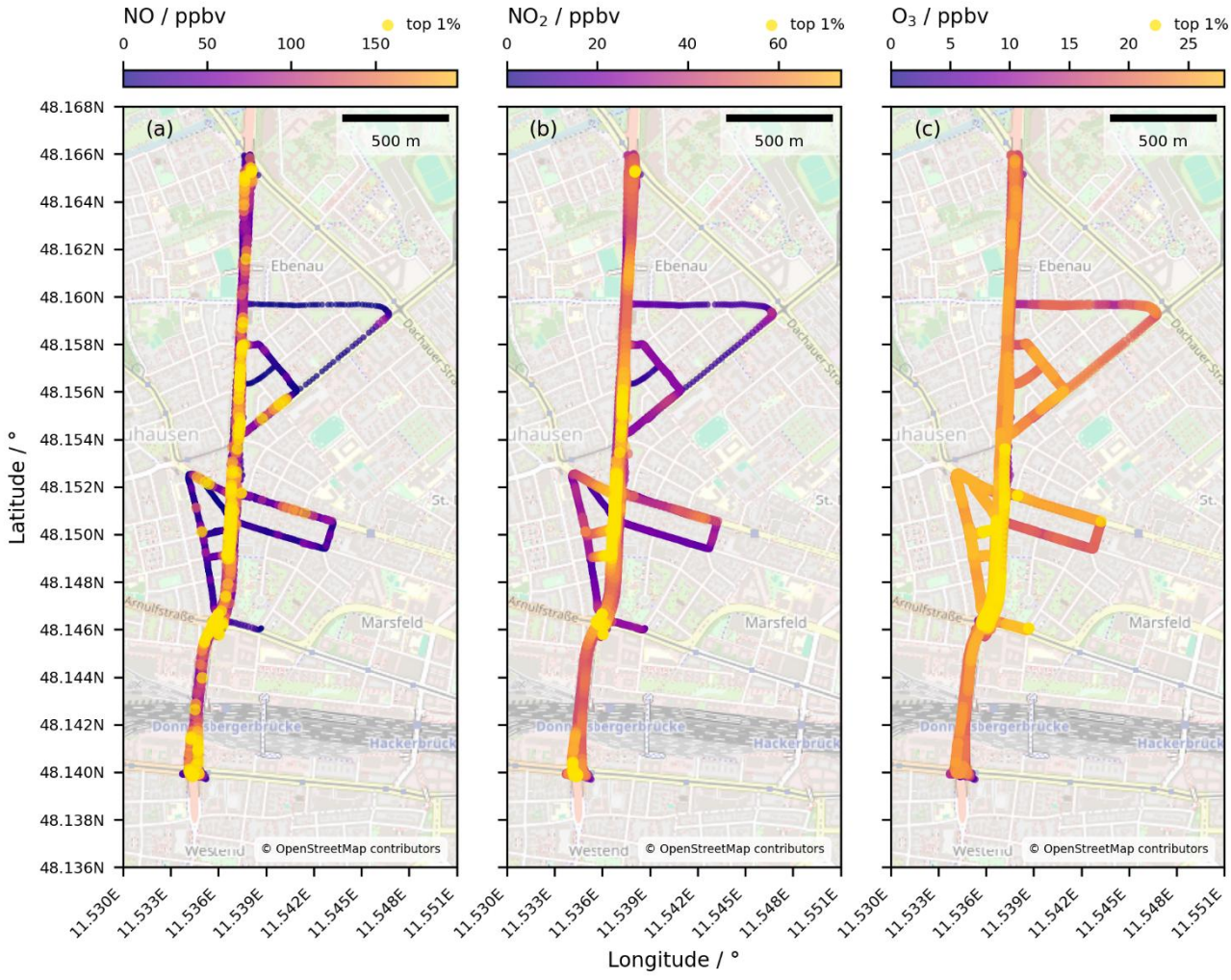



**Figure 3: Daytime spatial distribution of (a) NO, (b) $NO_2$, and (c) $O_3$ during September 10th – 18th 2023. Base maps from OpenStreetMap, distributed under the Open Data Commons Open Database License (ODbL) v1.0, https://www.openstreetmap.org/copyright.**

https://doi.org/10.5194/egusphere-2026-6529
Preprint. Discussion started: 2 November 2026
© Author(s) 2026. CC BY 4.0 License.

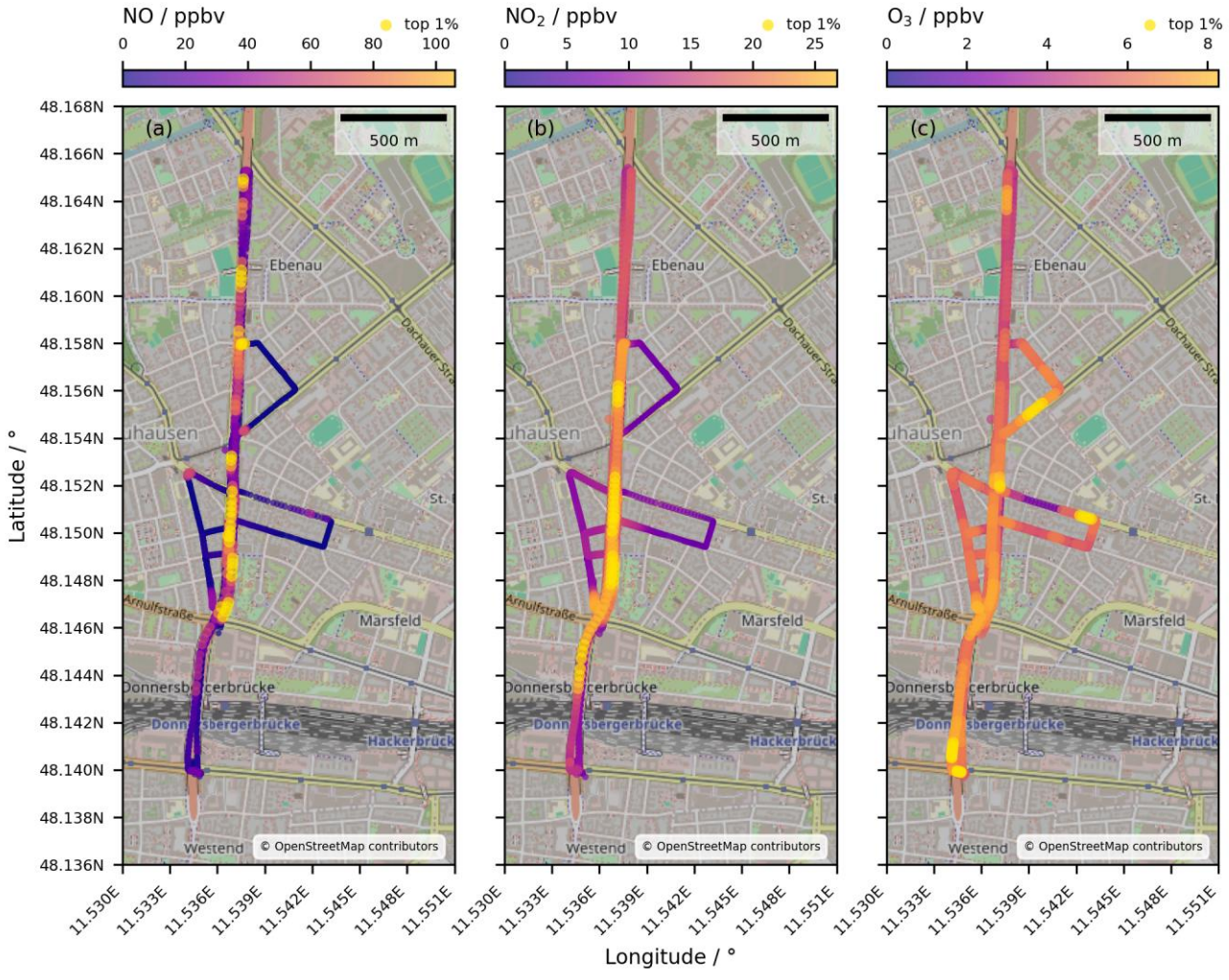



**Figure 4: Nighttime spatial distribution of (a) NO, (b) $NO_2$, and (c) $O_3$. Data are shown for the ride taking place on Friday, September 15th between 03:57 am and 05:57 am local time (D6R2R1R2R1R2R1R2R1R1, see Table S2 in Supplement). Note the different indexing of the colour scales compared to Figure 3. Base maps from OpenStreetMap, distributed under the Open Data Commons Open Database License (ODbL) v1.0, https://www.openstreetmap.org/copyright.**

https://doi.org/10.5194/egusphere-2026-6529
Preprint. Discussion started: 2 November 2026
© Author(s) 2026. CC BY 4.0 License.

### 3.2 VOC categorization and mixing ratio variation

In the following, we identify clusters of VOCs based on their spatial patterns and representative of their most likely sources. These analyses are primarily based on observations of the calibrated VOCs (Sect 3.2.1) and supported by patterns of a larger range of non-calibrated VOCs (Sect. 3.2.2).

#### 3.2.1 Clusters and patterns of calibrated VOCs

We first clustered and grouped all calibrated VOCs (as listed in Table 1) according to their spatial differences in order to investigate the characteristic VOC species and mixing ratios in the urban neighbourhood. The VOCs detected in the vicinity of the Landshuter Allee can be distinguished into three different categories with similar spatial patterns, as revealed from the hierarchical cluster analysis (Figure 5). The first category includes benzene, 2-methyl-2-pentene, toluene, *m*-diethylbenzene, *m*-xylene, and 1,2,3-trimethylbenzene. This category is very distinct from the other two, and assigned to traffic as a main source, since both alkenes and aromatics are known to be important constituents of vehicle exhaust (Schmitz et al., 2000; Wang et al., 2016b). The second category includes isoprene and α-pinene (monoterpenes), which are mainly of biogenic origin (Guenther et al., 2012; Hantson et al., 2017). The third category includes acetaldehyde, methanol, acetonitrile, and acetone. The main source of acetonitrile is biomass burning, but as a relatively inert compound, it can be transported over long distances and is therefore ubiquitous (de Gouw et al., 2003). Meanwhile, acetaldehyde, methanol, and acetone are all attributable to a multitude of sources, ranging from biogenic emissions to fuel burning and the atmospheric photooxidation of other VOCs (Heikes et al., 2002; Jacob et al., 2002; Millet et al., 2010). Hence, all these functionalized VOCs (defined in the following as VOCs possessing functional groups with heteroatoms) are less attributable to specific point sources in the study area.

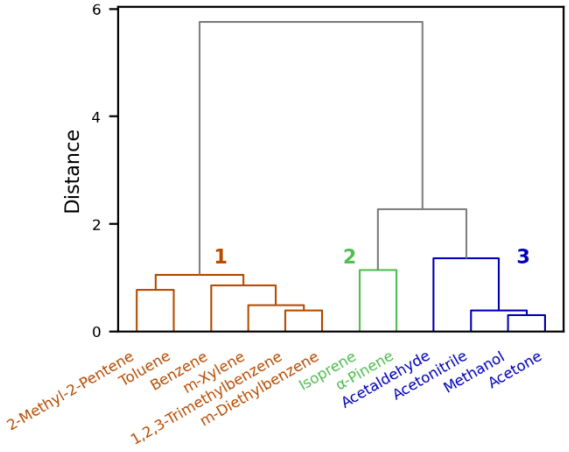



**Figure 5: Hierarchical clustering of VOCs, based on the normalized mean mixing ratios in the grid cells.**

This assignment of the VOC clusters to traffic or non-traffic sources was validated and supported by evaluating their spatial distribution in terms of distance from the main street (Figure 6b). Due to the North-South orientation of the Landshuter Allee,

https://doi.org/10.5194/egusphere-2026-6529
Preprint. Discussion started: 2 November 2026
© Author(s) 2026. CC BY 4.0 License.

the evaluation of the mixing ratios as a function of longitude essentially provides a cross-section in which the Landshuter Allee street canyon can be clearly distinguished from the surrounding area. Here, this analysis was carried out for latitudes between 48.1474°N and 48.1536°N (equivalent to 689 m). In this range, the Landshuter Allee is enclosed by tight infrastructure on either side, data for adjacent streets to the east and west are available, and the main street canyon can be constrained as being located at longitudes between 11.53615°E and 11.53775°E (Figure 6a). Both the $NO_x$ species and the VOCs of category 1 that were assigned to traffic-related sources show higher mixing ratios in the main street canyon than in the western and eastern neighbourhoods. No such pattern is observed for the biogenic and functionalized VOCs (categories 2 and 3) and for $O_3$, supporting the idea that sources other than traffic are dominant. Furthermore, substantial differences between the means and the medians are found for NO and the traffic-related VOC, indicating a non-Gaussian distribution and a large mixing ratio variability that probably results from the high proximity to the emission source.

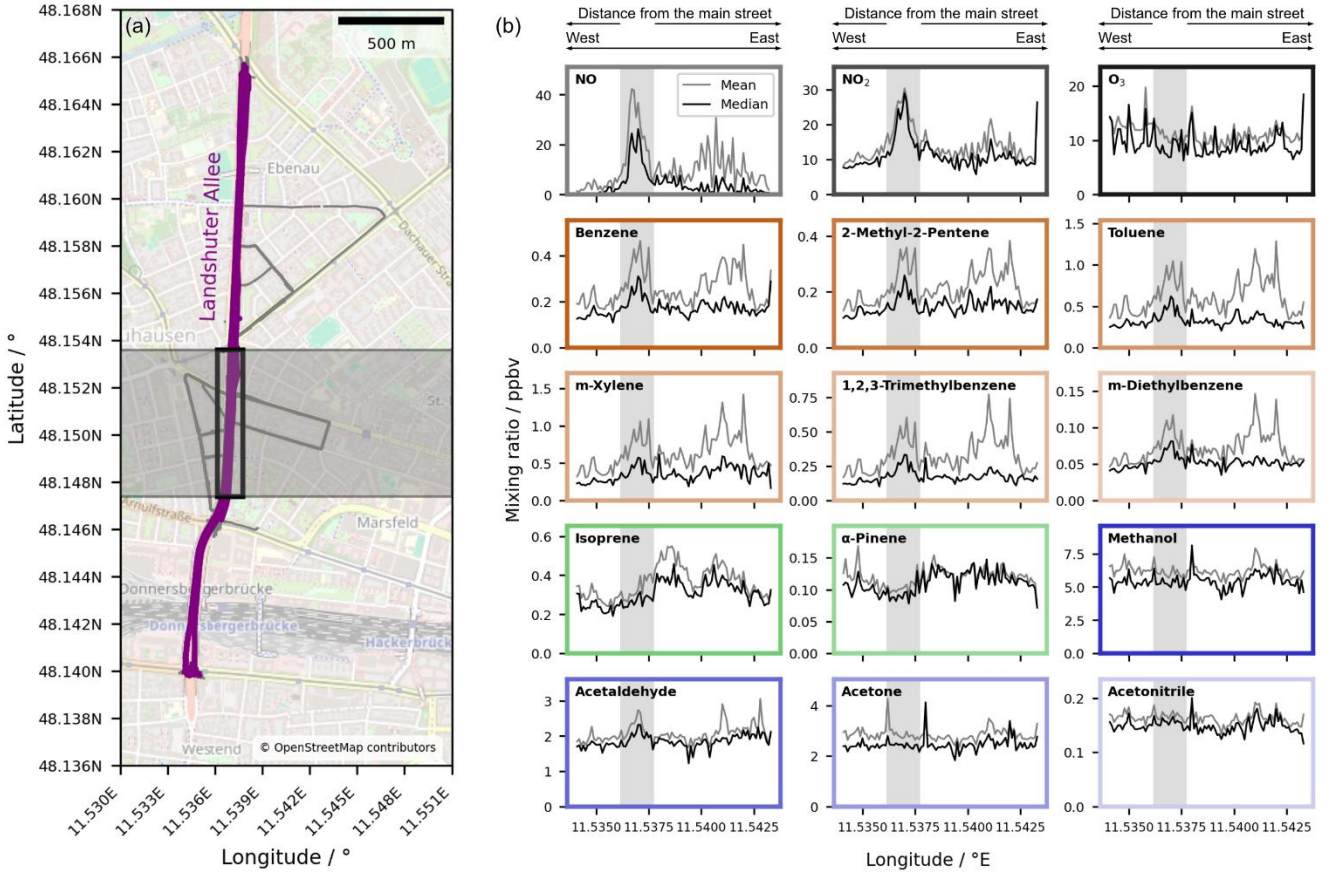
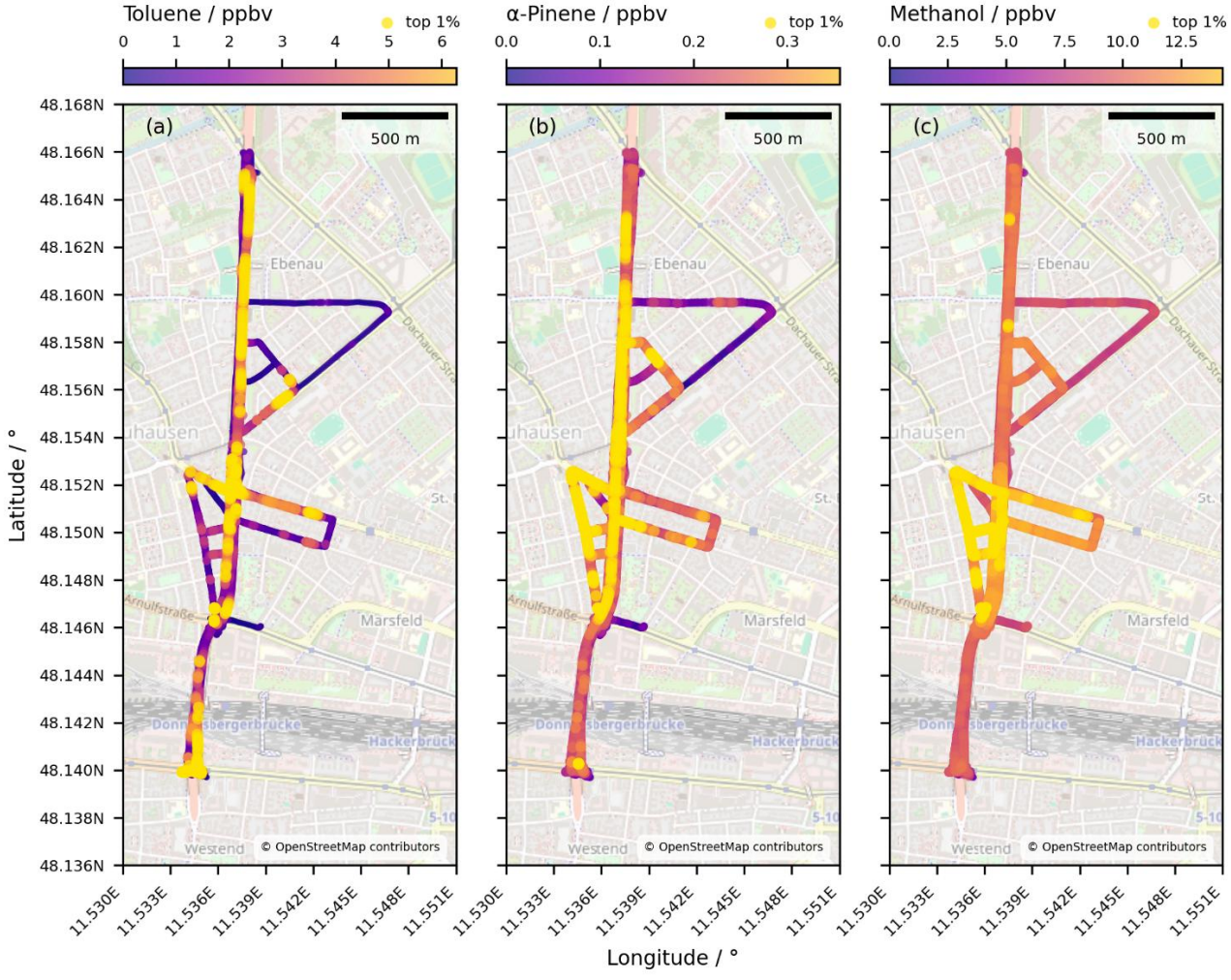



**Figure 6: VOC, $NO_x$, and $O_3$ mixing ratios in the main street canyon vs in adjacent streets. (a) Area selected to evaluate VOC, $NO_x$, and $O_3$ mixing ratios as a function of latitude. The grey area is the range over which the longitudinal cross-section was compiled (latitudes 48.1474°N – 48.1536°N). The black box represents the Landshuter Allee within that area (longitudes 11.53615°E – 11.53775°E). Base map from OpenStreetMap, distributed under the Open Data Commons Open Database License (ODbL) v1.0, https://www.openstreetmap.org/copyright. (b) Means and medians are as a function of longitude between 48.1474°N and 48.1536°N, equivalent to a west-east gradient. The shaded grey area represents the Landshuter Allee, and the x axis approximates the perpendicular distance from the main street, as shown in the upper axis label.**

https://doi.org/10.5194/egusphere-2026-6529
Preprint. Discussion started: 2 November 2026
© Author(s) 2026. CC BY 4.0 License.

340

The spatial VOC distribution at daytime is shown for toluene (Figure 7a), α-pinene (Figure 7b), and methanol (Figure 7c) as representative compounds for each of the VOC categories. Like NO and $NO_2$, toluene (average of 0.8 ± 1.6 ppbv; median 0.4 ppbv) occurred mainly on the Landshuter Allee and adjacent larger streets. The ambient mixing ratios of methanol (average of 6.3 ± 2.4 ppbv; median 5.7 ppbv) showed less spatial variations, peaking mainly in the western neighbourhood which is
345 characterized by a high density of restaurants and shops representing a mixed-use district. Lastly, the signal of α-pinene and other monoterpenes (average of 0.1 ± 0.1 ppbv; median 0.1 ppbv) peaked both along the Landshuter Allee and in the western neighbourhood. These hotspots are likely related to the presence of vegetation, as well as – for the lively western neighbourhood – emissions from restaurants/cafés as well as from humans (incl. personal care products).




350 **Figure 7: Daytime spatial distribution of (a) toluene, (b) α-pinene, and (c) methanol during September 10th - 18th 2023. Base maps from OpenStreetMap, distributed under the Open Data Commons Open Database License (ODbL) v1.0, https://www.openstreetmap.org/copyright.**

https://doi.org/10.5194/egusphere-2026-6529
Preprint. Discussion started: 2 November 2026
© Author(s) 2026. CC BY 4.0 License.

### 3.2.2 Suspect screening approach

The identified clusters can be validated further by evaluating the spatial patterns of a larger range of compounds. For this purpose, a large advantage of the utilisation of a PTR-ToF-MS is the fast acquisition of entire mass spectra. These mass spectra can be evaluated in retrospect to identify prevalent airborne VOC (Table S1, Supplement). Without calibration standards, the quantification of these compounds can be performed based on the PTR-ToF-MS transmission curve, yet with larger uncertainties than when identified and calibrated with a standard gas. Therefore, we evaluated these compounds on a purely qualitative basis. A statistical approach to the spatially resolved data including both calibrated and non-calibrated compound can not only substantiate the source appointment of the calibrated VOCs given that the sources of the non-calibrated compounds are already known, but also allows for a more comprehensive interpretation of the origin of non-calibrated compounds and for a higher degree of certainty in the assignment of the peaks in the mass spectrum.

We demonstrate the application of this approach in Figure 8, where we performed the hierarchical cluster analysis (Figure 5) with a wider range of VOCs, including both calibrated and non-calibrated compounds. Amongst the calibrated VOCs, the same compounds (traffic-related / biogenic / functionalized) are still grouped together, with the largest difference persisting between traffic-related compounds on the one hand and biogenic and functionalized compounds on the other hand. Some non-calibrated VOCs group relatively closely with the calibrated traffic-related VOCs, namely d4-siloxane, d5-siloxane, ethanol and naphthalene. Naphthalene and ethanol are known to be directly emitted from traffic (de Abrantes et al., 2004; Dunmore et al., 2016). In contrast, siloxanes are predominantly associated with consumer and personal care products but there is evidence to suggest that passengers who have previously used siloxane-containing products may emit these compounds into the vehicle cabin from where they can then be vented out and mix with exhaust emissions (Coggon et al., 2018; Gkatzelis et al., 2021).

For the large cluster containing both biogenic and functionalized VOCs, non-calibrated compounds include sesquiterpenes, acetic acid, acrolein, isoprene oxidation products (MVK+MACR+ISOPOOH), phenol, cresols, dimethyl sulfide, benzaldehyde, furan, MEK, formaldehyde, and methylglyoxal. With the exception of dimethyl sulfide and sesquiterpenes, both of which are known to be emitted by vegetation (Duhl et al., 2008; Geng and Mu, 2006), all of these compounds possess oxygen-containing functional groups, so that photochemical production from other VOC precursors within the ambient air is a possible source. Within the compounds assigned to the class of functionalized VOCs, two subgroups can be distinguished. Atmospheric processing is likely the main source for acrolein, acetaldehyde, MVK+MACR+ISOPOOH, phenol, and cresols, whereas primary emissions such as from the breath or skin of humans may be a significant contribution for acetonitrile, acetone, methanol, and acetic acid (Jordan et al., 1995; Wang et al., 2022).

Generally, an exact distinction between the biogenic cluster and the functionalized cluster is difficult. For instance, the group containing dimethyl sulfide, benzaldehyde, furan, MEK, formaldehyde, and methylglyoxal is only marginally more similar to

https://doi.org/10.5194/egusphere-2026-6529
Preprint. Discussion started: 2 November 2026
© Author(s) 2026. CC BY 4.0 License.

the pre-identified biogenic VOCs (isoprene, a-pinene / monoterpenes) than to the pre-identified functionalized VOCs (distance of 2.13 vs 2.40). This may be caused by the presence of mixed sources (especially so since functionalized VOCs have mixed sources to begin with), or the diffuse character of both biogenic sources and photooxidation (as an exemplary source of functionalized compounds) within the study area. Furthermore, different reactivities are likely to cause differences in the dispersion and spatial patterns of compounds originating from the same or similar sources, limiting the applicability of approaches such as hierarchical cluster analysis or positive matrix factorisation if not accounted for (Yuan et al., 2012). This could explain the unique position of the sesquiterpenes, even though one would expect a similar origin as for the monoterpenes. Isomers of monoterpenes or sesquiterpenes can differ in their reactivity by several orders of magnitude, respectively (Isaacman-VanWertz et al., 2024), hence the specific isomeric composition could be decisive for their atmospheric losses.

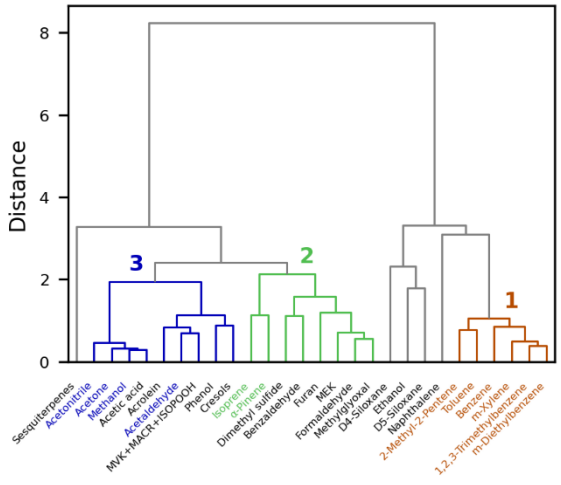



**Figure 8: Hierarchical clustering of VOCs, based on the normalized mean mixing ratios in the grid cells and including both calibrated (coloured font) and non-calibrated (black font) compounds. The group numbers reflect the previously identified groups from Figure 5.**

Even without considering reactive losses, compounds that were mainly attributable to traffic emissions could be clearly distinguished from those that were mainly attributable to non-traffic sources. For studies with a similar setup and with similar prerequisites, hierarchical cluster analysis based on averaged grid cell mixing ratios hence appears as a promising tool also for non-target analysis and suspect screening. As a quantitative analysis of the non-calibrated compounds is not possible, and because a full profiling of the VOC pool is unrealistic in all cases, the following analyses are restricted to the calibrated VOCs. Still, the persistence of the previously identified clusters even when more species are taken into account and the fact that the non-calibrated VOCs fall into the expected categories support our interpretation of the three clusters (traffic-related / biogenic / functionalized) discussed above.

https://doi.org/10.5194/egusphere-2026-6529
Preprint. Discussion started: 2 November 2026
© Author(s) 2026. CC BY 4.0 License.

### 3.3 Spatial heterogeneity and clustering of grid cells

With the ultimate goal of defining focus areas for further characterization (Sect. 3.4), we aimed at characterizing spatial patterns within the study area. To do so, we evaluated (Sect. 3.3.1) and subsequently mapped and compared (Sect. 3.3.2) the outputs of the hierarchical cluster analysis, the k-means analysis, and the NMDS analysis. Notably, these analyses all represent different dimensions of the dataset: the hierarchical cluster analysis encompasses all organic and inorganic species and is predominantly influenced by compounds with significant spatial differences; the k-means analysis was designed to reveal different regimes as defined by the prevalence of inorganic species; and the NMDS analysis was used to classify grid cells according to their association with the VOCs.

#### 3.3.1 Results of hierarchical clustering, k-means, and NMDS

First, both the hierarchical cluster analysis and the k-means analysis provided a direct approach to group the grid cells. The hierarchical cluster analysis of the grid cells revealed two main groups, shown in different shades of violet and turquoise (Figure 10a). Each group is further divided into two subgroups, as illustrated by darker and lighter tones. In itself, the outcome of the hierarchical cluster analysis does not readily lend itself to interpretation and must be translated onto the map prior to further assessment (see below). In contrast, the k-means analysis shows no obvious clustering of grid cells but provides contextual information (Figure 10b). The lack of distinct groups can be attributed to the geographic continuity of the grid cells (Kreft and Jetz, 2010), which in turn is characterized by the existence of transition zones that are affected by blending and transportation of compounds (here: $NO_x$ and $O_3$) through the street networks. Rather than showing sharply defined groups, the k-means algorithm essentially results in the classification of the grid cells as a function of the ambient $NO_x$ mixing ratio.

A limitation of both above-mentioned approaches is their inability to resolve dependencies across the full set of measured compounds. Therefore, we used NMDS to better evaluate spatial differences relating to the distribution of all quantified species, including the individual VOCs. While NMDS is traditionally an ordination and visualisation method, here it was used to assess the relationship between distinct grid cells and spatial patterns of the measured species, particularly the VOCs. In the graphical representation of the NMDS analysis (Figure 9), both the grid cells (points) and the measured compounds (vectors) are displayed in a two-dimensional space. The two NMDS dimensions (NMDS1 and NMDS2) are abstract and have no physical meaning. Instead, they reflect the similarity or dissimilarity between the original high-dimensional data. Close proximity of the points is indicative for a high similarity of the grid cells with regard to the prevalence and variability of the compounds included in the analysis. The direction and length of the vectors represent the degree to which these compounds define and are defined by the two NMDS dimensions. Alignment between vectors suggests a positive correlation between the respective compounds.

https://doi.org/10.5194/egusphere-2026-6529
Preprint. Discussion started: 2 November 2026
© Author(s) 2026. CC BY 4.0 License.

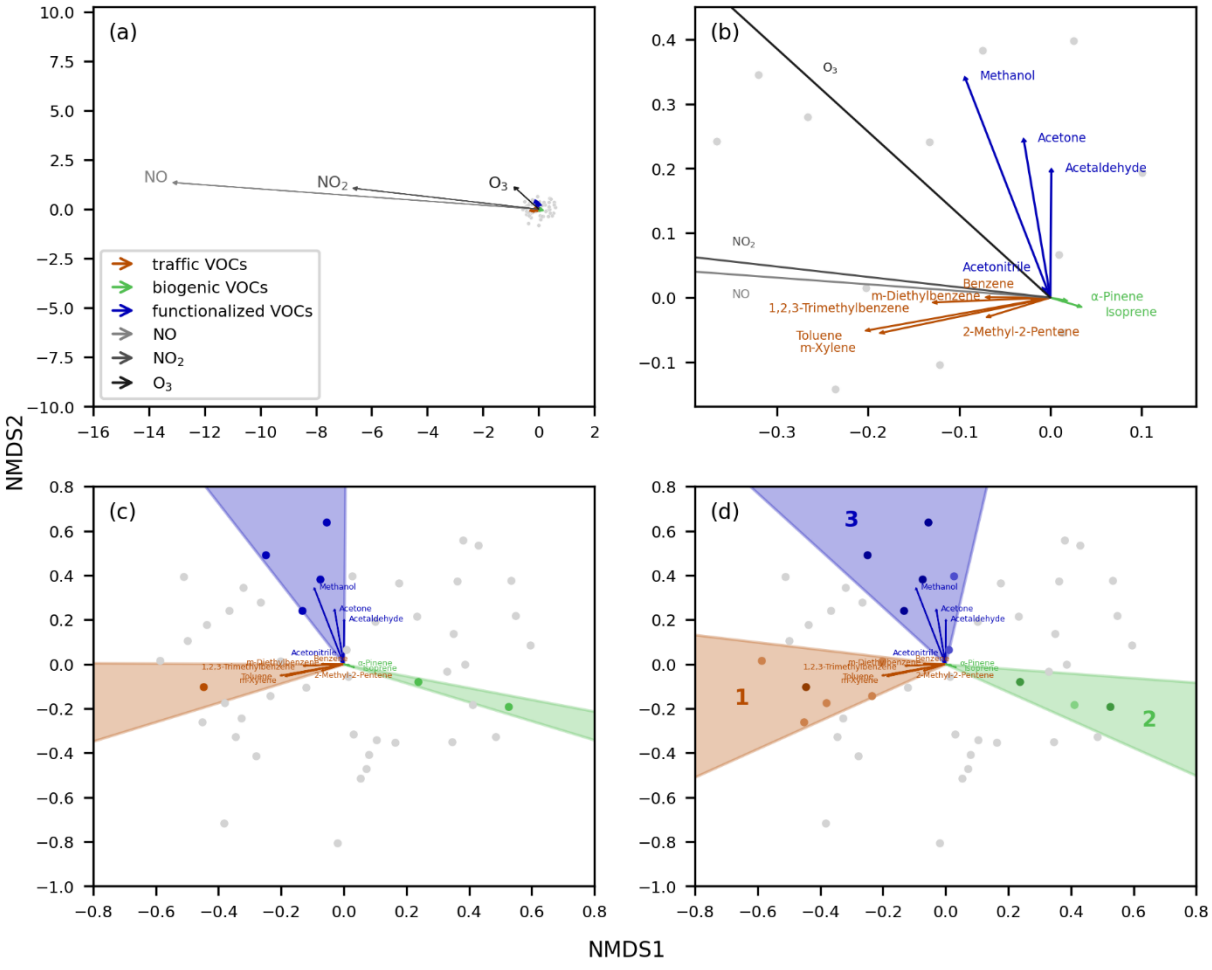



**Figure 9: NMDS results based on the normalized data of all calibrated gas-phase species, showing (a) all included compounds in the two-dimensional space, (b) a close-up view on the VOCs, (c) the areas and associated grid cells spanned by the three VOC categories, and (d) an expanded assignment (area + 10° on either side) of the grid cells to the three VOC categories. In panel (d), the grid cells are coloured in a darker shade if they have been included in the core assignment as shown in panel c, and in a lighter shade if they are only included in the extended assignment. The VOC categories are identical to those in Figure 5. Note that while the axes limits and scales differ between panels, the aspect ratio remains the same.**

Out of all included species, NO, $NO_2$, and $O_3$ display the strongest associations with the NMDS axes as expressed by their vector lengths (Figure 9a). This is mainly true for NMDS1, although they also retain longer vectors than any of the VOCs on NMDS2. The vector length is likely caused by their high heterogeneity along both spatial and temporal dimensions, with very sharp differences between grid cells. Within the same ordination, the calibrated VOCs can be grouped into categories according to the alignment of their vectors (Figure 9b). Here, we identified and hence confirmed the same three distinct categories as in the hierarchical cluster in Figure 5. The vectors of the compounds in the first VOC category, composed of aromatics and

https://doi.org/10.5194/egusphere-2026-6529
Preprint. Discussion started: 2 November 2026
© Author(s) 2026. CC BY 4.0 License.

alkenes, point into a similar direction as the NO and $NO_2$ vectors, supporting the previous assignment of these compounds as traffic-related VOCs. Secondly, α-pinene (monoterpenes) and isoprene are grouped together. While the NMDS does not offer additional information as to their origin, it also does not contradict the assignment as predominantly biogenic VOCs and shows a clear difference from the other compounds. The third VOC category was previously assigned to functionalized compounds. In the NMDS, their orientation is similar to $O_3$, which could indicate a high relevance of photochemical production.

In the two-dimensional NMDS space, the locations do not fall into distinct clusters, arguably because the individual grid cells are adjacent and therefore contain mixed and transitional areas, in a similar manner as for the k-means analysis. However, the identified VOC categories can aid the interpretation of the spatial characteristics. In Figure 9c, the areas spanned by the vectors associated with the VOCs of any given VOC category are highlighted. As these areas only cover a few grid cells, they were expanded by 10° on either side to for a less conservative assignment (Figure 9d). The areas that are only included in this slightly extended assignment are shown in a different colour shade for differentiation. Using the described approach, the grid cells most influenced by a given VOC group can be identified as such. By classifying the grid cells according to their association with the VOC categories, the NMDS is essentially used as a clustering method as well.

### 3.3.2 Side-by-side comparison and interpretation of spatial patterns

We conducted a cross-comparison of the results and the spatial information of all statistical analyses including the hierarchical clustering (mapped in Figure 10c), the k-means analysis (mapped in Figure 10d), and the NMDS (mapped in Figure 10e). In case of the hierarchical cluster analysis outcome, the grid cells in different shades of turquoise occur exclusively in the neighbourhood to the west and east of the Landshuter Allee, while the dark and light violet grid cells are mostly found along the main street canyon (Figure 10c). This sharp distinction between the street canyon and the neighbourhood points to a high influence of traffic-related compounds (the allocated VOCs as well as NO and $NO_2$) on the clustering, driven by their distinct spatial heterogeneity. This interpretation is supported by the results of the k-means analysis (Figure 10d), where the high-$NO_x$ grid cells are prevalent in the main street canyon, whereas low-$NO_x$ grid cells occur in the neighbourhoods. The high resemblance of the spatial patterns revealed by these two clustering approaches support a large impact of $NO_x$ on both analyses. The spatial representation of the NMDS classification (Figure 10e), in turn, results in a less comprehensive spatial characterisation compared to the cluster analyses but highlights areas with the most distinct VOC fingerprint. In general, the VOC-based NMDS shows and confirms that the most heavily traffic-influenced areas occur along the Landshuter Allee as well as on a larger adjacent street. Particularly, the area around the LFU monitoring station (see Figure 1b) stands out, which has been shown to experience a relatively low mixing intensity (as indicated by the turbulent kinetic energy, TKE) for various synoptic wind directions compared to the rest of the street canyon (Sungur et al., 2026). In contrast, areas that are characterized predominantly by the variability of biogenic emissions occur only in the neighbourhoods. Areas that are largely influenced by functionalized VOCs are found both along the large streets and in the neighbourhoods, indicating the presence of mixed sources and/or effective atmospheric oxidation processes.

https://doi.org/10.5194/egusphere-2026-6529
Preprint. Discussion started: 2 November 2026
© Author(s) 2026. CC BY 4.0 License.

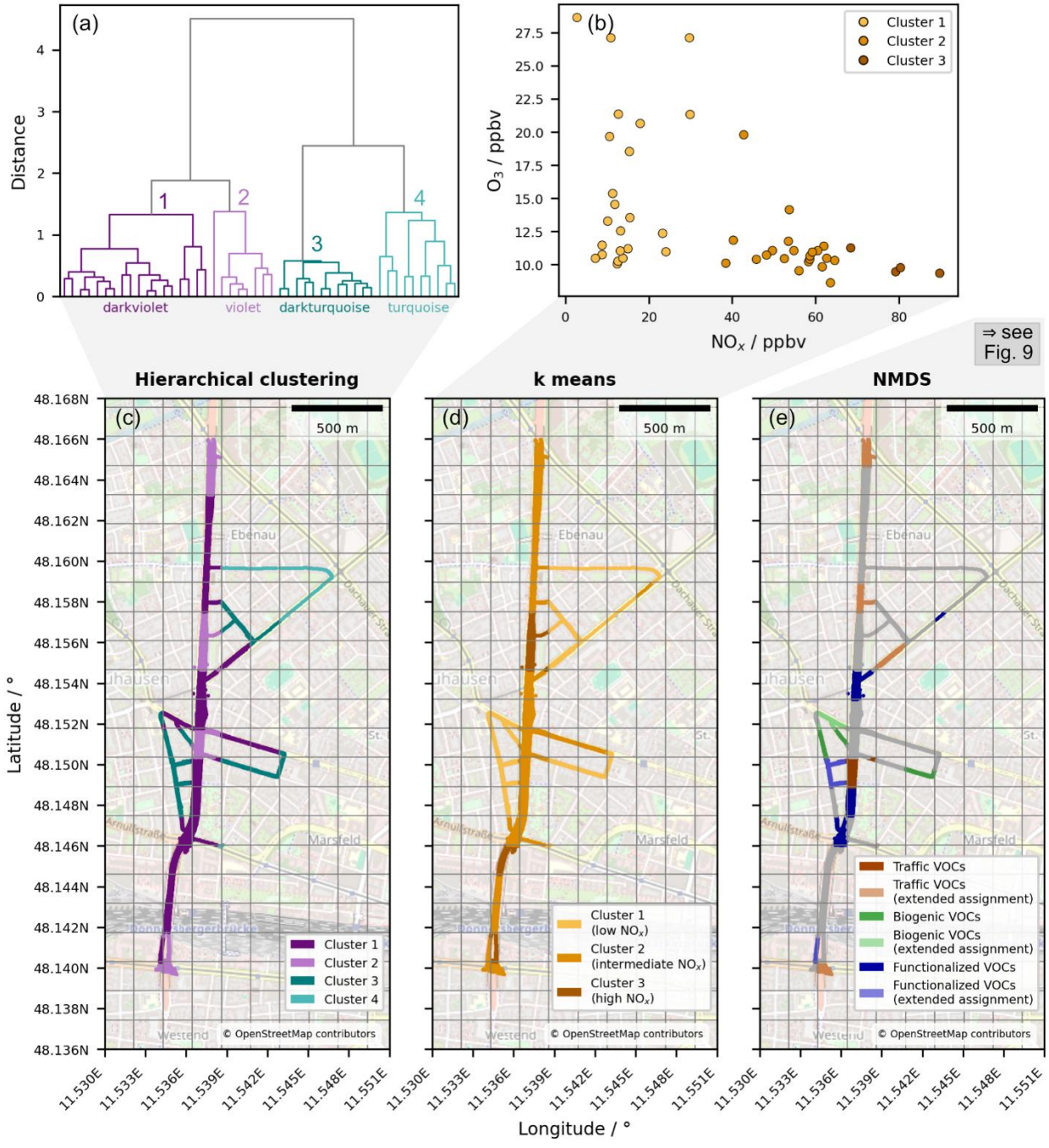



**Figure 10: Spatial differences between the grid cells based on different statistical analyses. (a) Results of hierarchical clustering of the grid based on the normalized mean mixing ratios of VOCs, $NO_x$, and $O_3$ in the grid cells. (b) Results of the k-means analysis of the grid cells. (c) Mapping of the hierarchical clustering results. (d) Mapping of the k-means results. (e) Mapping of the NMDS results (as originally presented in Figure 9). Dark colour shades represent the core assignment (Figure 9c), whereas light colour shades represent the extended assignment (Figure 9d). Base maps from OpenStreetMap, distributed under the Open Data Commons Open Database License (ODbL) v1.0, https://www.openstreetmap.org/copyright.**

https://doi.org/10.5194/egusphere-2026-6529
Preprint. Discussion started: 2 November 2026
© Author(s) 2026. CC BY 4.0 License.

### 3.4 VOC fingerprints and their impact on air quality

To evaluate how spatial differences in ambient concentrations of gaseous species impact the ambient air quality, we aimed at defining distinct focus areas within the overall study area. As the statistical analyses (Sect. 3.3, Figure 10) revealed a clear difference between the Landshuter Allee street canyon and each of the surrounding neighbourhoods, these two neighbourhoods were selected as focus areas accordingly. Additionally, we included five areas along the Landshuter Allee itself to distinguish between intersections, areas with varying (infra-)structural density, and the Landshuter Allee tunnel. The final selection hence consisted of seven focus areas (Figure 11a):

1. Landshuter Allee, intersection with Dachauer Straße.
2. Landshuter Allee, north of the tunnel, dense infrastructure with pronounced canyon-like structure.
3. Landshuter Allee tunnel. In the statistical analysis of the grid cells above, the tunnel is difficult to distinguish, as the coordinates overlap with those of the aboveground street. Still, we wanted to single out the tunnel for the following analyses, as we expected distinct characteristics due to the restricted airflow and the absence of light. Area #3 therefore refers to the belowground measurements exclusively, manually filtered in the dataset accordingly.
4. Landshuter Allee, south of the tunnel, dense infrastructure with pronounced canyon-like structure.
5. Landshuter Allee, freely exposed and unconfined area north of and above the bridge Donnersberger Brücke.
6. Western Neighbourhood.
7. North-Eastern Neighbourhood.

The mixing ratio distributions for all calibrated compounds are shown as boxplots for each of the seven focus areas in Figure 11b. The traffic-related VOCs, and in particular NO and $NO_2$, are all more abundant along the Landshuter Allee (#1 – #5) than in the surrounding neighbourhoods (#6 and #7), with the medians being higher by factors of 1.6 to 2.1 for the VOCs, 3.3 for $NO_2$, and 58.0 for NO (factors calculated for each compound as the average medians in areas #1 – #5 compared to the average medians in areas #6 and #7). Especially for the traffic-related VOCs, the highest average mixing ratios are found in the tunnel (#3), being by a factor of 1.4 to 1.7 higher than in the other areas along the Landshuter Allee. While the source strength in the tunnel should be similar to other parts of the street canyon, there is much less dilution due to poor ventilation and the relatively small air volume into which compounds are emitted, leading to accumulation. Additionally, the absence of sunlight means that photochemical sinks are less effective than aboveground, which agrees with the observation that the tunnel doesn't display such noticeably higher mixing ratio for NO and $NO_2$ which – in comparison to the VOCs – are mainly cycled rather than photochemically degraded. For the traffic-related VOCs, the tunnel is further characterized by the large spread in the collected data as well as asymmetry and non-Gaussianity with the mean being by factors between 1.3 and 1.6 higher than the median. This can point towards heterogenous conditions rather than a single stable regime, and – due to the reduced sink strength – to a strong coupling of the mixing ratios to the source strength, i.e. the traffic volume.

https://doi.org/10.5194/egusphere-2026-6529
Preprint. Discussion started: 2 November 2026
© Author(s) 2026. CC BY 4.0 License.

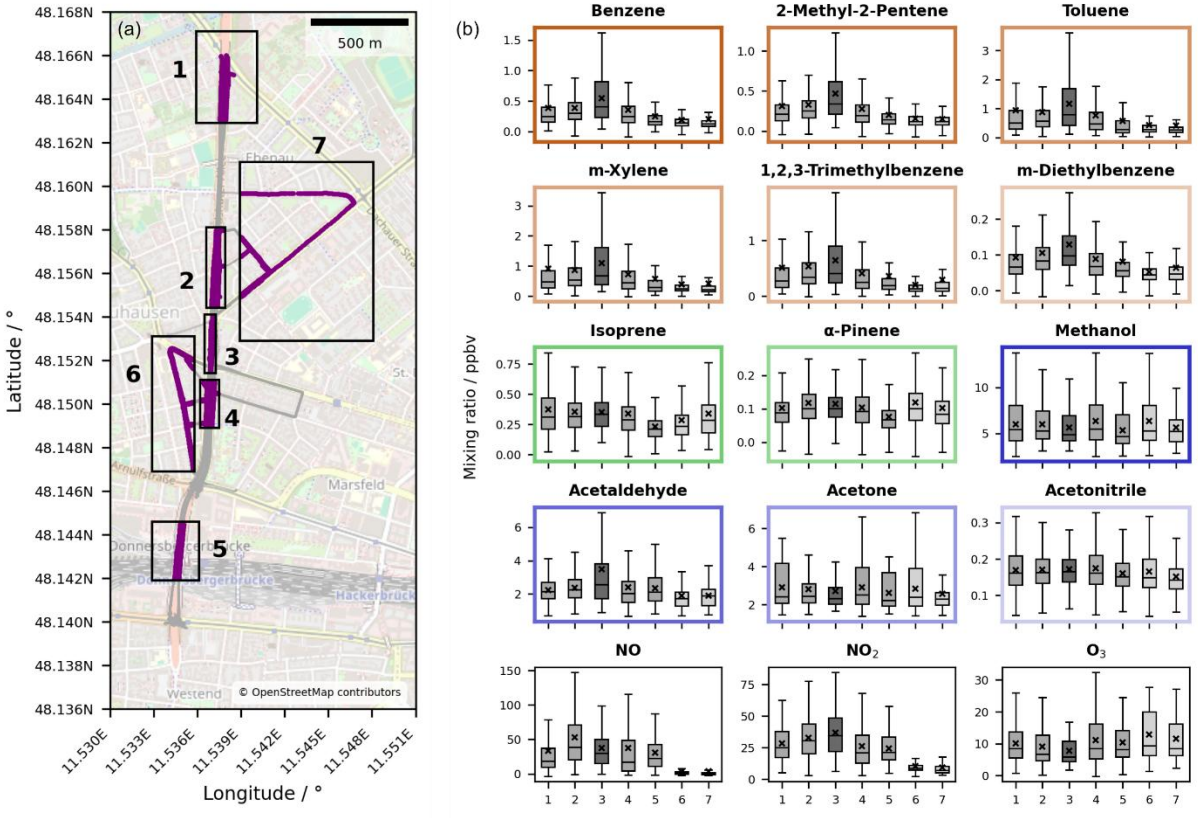



**Figure 11: VOC distribution in focus areas. (a) Definition of the seven focus areas. Base map from OpenStreetMap, distributed under the Open Data Commons Open Database License (ODbL) v1.0, https://www.openstreetmap.org/copyright. (b) Mixing ratios of each of the calibrated compounds within these focus areas. In the boxplots, the grey scales of the boxes represent the neighbourhoods (#6, #7; light grey), the aboveground areas along the Landshuter Allee (#1, #2, #3, #4; medium grey), and the Landshuter Allee tunnel (#3; dark grey).**

Such distinct spatial patterns are missing for the other VOCs (biogenic and functionalized) and $O_3$, with the medians between areas #1 to #5 vs areas #6 and #7 differing only within factors of 1.0 to 1.2 for the VOCs and by a factor of 0.8 for $O_3$. For the biogenic VOCs, this may be explained by the extensive tree cover across the study area except for within the Landshuter Allee tunnel, slow and continuous release, and effective dispersion and transport. In case of the functionalized VOCs, atmospheric aging and transport from distant sources are generally expected to dominate over any direct point sources. For acetaldehyde in particular, there is a similar yet much less pronounced pattern as for the traffic-related compounds, with elevated mixing ratios and high variability in the street canyon and especially in the tunnel. This suggests a noticeable contribution of vehicle exhaust to the acetaldehyde mixing ratio, which is in line with previous studies (Corrêa et al., 2003). For $O_3$, the mean mixing ratios are lowest in the tunnel (7.7 ppbv) and highest in the neighbourhoods (12.8 ppbv and 11.6 ppbv), which would suggest that $NO_x$ is a sink rather than a source of $O_3$ in the study area and that the photochemical $O_3$ production is strongly VOC-limited.

https://doi.org/10.5194/egusphere-2026-6529
Preprint. Discussion started: 2 November 2026
© Author(s) 2026. CC BY 4.0 License.

For all VOCs, both the medians and the means of the mixing ratios are by factors of up to 1.3 higher in the street canyon north and south of the tunnel (#2 and #4) than at the intersection (#1) and the open area above the Donnersbergerbrücke (#5), likely resulting from a reduced sink strength due to the constrained architecture of the Landshuter Allee and poor mixing. Additionally, since the tunnel is equipped with a wall separating the different directions of travel, the moving vehicles create a flow of air that can transport the traffic-dominated air from the tunnel to the outside (Figure S4, Supplement).

Using the mean VOC mixing ratios for each focus area, these areas can be further characterized with regard to typical air quality parameters and photochemical indicators, as introduced in Sect. 2.5. To evaluate the contribution of the different VOCs to each of the sum parameters, we averaged the data for each focus area across all the different rides, as displayed on the stacked bar plots in Figure 12. Additionally, to better consider the temporal dynamics of the spatial differences of the air quality parameters, we calculated these parameters for each ride separately, as visualized by the boxplots in Figure 12. Taking the resulting spread of the numerical values into account, group differences between the focus areas were then analysed using the Mann-Whitney U test. We acknowledge that uncertainties are propagated from uncertainties of the measured data and of the literature values used to calculate the parameters and indicators. Both sources of uncertainties are systematic across the different locations, sustaining comparability. Further limitations of this approach exist in terms of incomplete VOC profiling. However, since absolute values are needed for these calculations and since mixing ratios derived for uncalibrated VOCs are highly uncertain, it is methodologically more robust to restrict these analyses to the calibrated VOCs. Also, complete coverage of the VOC pool can never be guaranteed, even when including non-calibrated VOCs.

Across the study area, the relative distribution of the VOC mixing ratios shows the functionalized VOCs as the largest fraction, followed by traffic-related VOCs and biogenic VOCs (Figure 12a). The oxygenated compounds methanol, acetaldehyde, and acetone are most abundant, jointly accounting for 73% to 86% of the measured VOC load. This is in agreement with other studies showing a dominance of oxygenated VOCs in urban air (Karl et al., 2018; Wu et al., 2020). The functionalized compounds also contribute to the OFP (24% to 37%) and the OH radical reactivity (26% to 36%). As the VOC composition is dominated by the functionalized VOCs which are distributed rather ubiquitously, the sum mixing ratio of the VOCs does not differ significantly between any of the locations.

In contrast, and due to spatial variations of the less abundant but more reactive traffic-related VOCs and biogenic VOCs, the calculated oxidant reactivities and potentials for secondary pollutant formation do show statistically significant spatial patterns. Especially the traffic-related VOCs have a substantial spatial variability and are more abundant in the street canyon and the tunnel compared to the neighbourhood (Figure 11b). Even though they do not contribute substantially to the VOC sum (11% to 25%), they are important with regard to the ambient SOAP (Figure 12b, contribution between 84% and 94%), OFP (Figure 12c, contribution between 49% and 66%), OH radical reactivity (Figure 12d, contribution between 31% and 49%), and $O_3$ reactivity (Figure 12e, contribution between 82% and 93%). The SOAP is mainly related to the oxidation of toluene, whereas

https://doi.org/10.5194/egusphere-2026-6529
Preprint. Discussion started: 2 November 2026
© Author(s) 2026. CC BY 4.0 License.

the $O_3$ reactivity is largely attributable to 2-methyl-2-pentene. Given the fast addition of $O_3$ to the double bond of alkenes, it is likely that further alkenes from traffic emissions make up an additional substantial sink for $O_3$. Biogenic VOCs are even less abundant (contribution of 2% to 4% to the total VOC mixing ratio), but are relevant for the OH radical reactivity (Figure 12d, contribution between 21% and 37%) and dominate the $NO_3$ radical reactivity almost completely (Figure 12f, contribution of 99% in all focus areas).

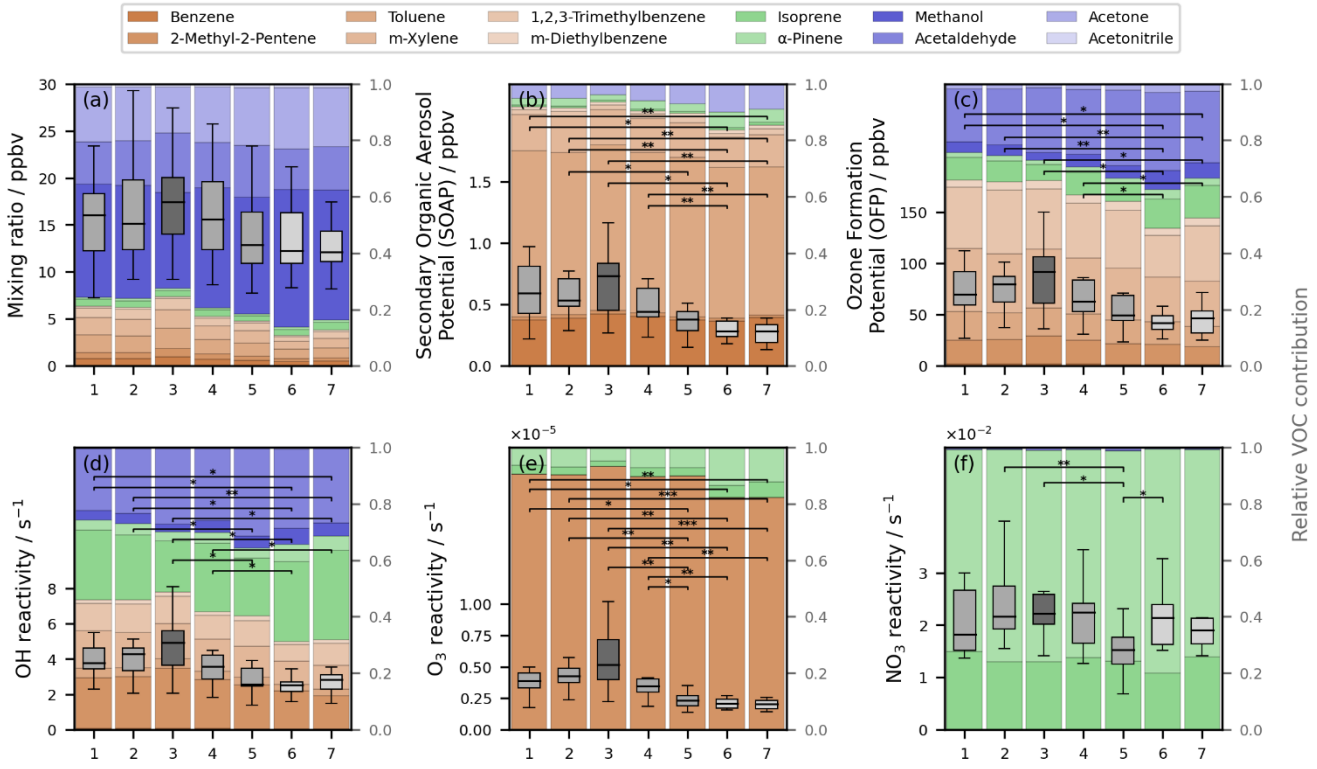



**Figure 12: Average VOC distribution and impact on air quality for the different focus areas. Subplots show (a) mixing ratios, (b) SOA formation potentials, (c) $O_3$ formation potentials, (d) OH radical reactivities, (e) $O_3$ reactivities, and (f) $NO_3$ radical reactivities. To illustrate the temporal variability of the spatial differences of these parameters, the boxplots represent the distribution of the average sum parameters across the 12 different rides (Table S2, Supplement). Group differences were analysed using the Mann-Whitney U test. Significance levels are denoted as * = $p < 0.05$, ** = $p < 0.01$, and *** = $p < 0.001$. The grey scales of the boxes represent the neighbourhoods (#6, #7; light grey), the aboveground areas along the Landshuter Allee (#1, #2, #3, #4; medium grey), and the Landshuter Allee tunnel (#3; dark grey).**

Across these parameters, some general rules apply in terms of spatial characteristics. Firstly, focus areas #6 and #7 (west and east neighbourhoods) never differ significantly from one another. The same is true for focus areas #1, #2, #3, and #4 (Landshuter Allee street canyon north and south of the tunnel, tunnel, and Northern intersection). Although the highest SOAP, OFP, OH reactivity, and $O_3$ reactivity are found in the tunnel, the temporal spread in these values appears to be large enough

https://doi.org/10.5194/egusphere-2026-6529
Preprint. Discussion started: 2 November 2026
© Author(s) 2026. CC BY 4.0 License.

to make the tunnel statistically indistinct from the aboveground street. Secondly, the most prevalent and significant differences are generally found between the neighbourhoods (#6 and #7) and the main street or tunnel (#1 – #4). With the exception of the α-pinene–dominated $NO_3$ reactivity, area #5 (bridge over railways) appears to be more similar to the neighbourhoods than to the remaining part of the Landshuter Allee. While the main street canyon is confined by the surrounding infrastructure which restricts air mixing (Sungur et al., 2026), no such infrastructure is present alongside the bridge. Therefore, it is likely that emissions are diluted more effectively, which in turn causes the VOC mixing ratios and impacts to approach those found in the neighbourhoods where the source strength is reduced.

Noteworthily, the median OFP (Figure 12c) exceeds 40 ppbv in all focus areas and even approaches 100 ppbv in the tunnel. This observation is in contrast with the observed spatial pattern and the low mixing ratios of $O_3$ (Figure 3). A likely explanation for this discrepancy is the effective $O_3$ titration, by ambient VOCs, NO, and $NO_2$. This chemical sink for $O_3$ is the most pronounced in the tunnel (Figure 12e), explaining why mixing ratios of $O_3$ are lowest in the tunnel even though the OFP is highest. Additionally, the production of $O_3$ from both $NO_2$ photolysis and VOC photooxidation is limited in the tunnel due to absence of radiation, further limiting the capacity of the air mixture to reach its full potential for $O_3$ production.

The MIR values that we used to calculate the OFP are a worst-case estimate and valid for high-$NO_x$ conditions where $O_3$ production is VOC-limited. To constrain the sensitivity of ambient $O_3$ production to either VOCs or $NO_x$, Kirchner et al. (2001) have proposed an indicator θ that describes the OH radical fate and is defined as the ratio of the $NO_x$ OH reactivity ($k_{OH}^{NOx}$, $s^{-1}$) to the VOC OH reactivity ($k_{OH}^{VOC}$, $s^{-1}$). Values of $\theta > 0.2$ indicate VOC-limited conditions, whereas values of $\theta < 0.01$ are associated with a high sensitivity towards changes in ambient $NO_x$ (Kirchner et al., 2001). We calculated the OH reactivities as shown in Eq. 1, using the rate coefficients for the reactions with OH radicals as listed in Table S3 (Supplement). For the VOC OH reactivity, we only took into account the calibrated compounds, but acknowledge that more contributing compounds exist. The $NO_x$ OH reactivity exceeds the VOC OH reactivity in all focus areas, resulting in values of θ way above 0.2 and indicating that the entire area around the Landshuter Allee is strongly VOC-limited with regard to $O_3$ production. This is especially the case in the street canyon and the tunnel which are heavily $NO_x$-saturated with values in the range of $\theta = 4.0 – 5.7$, whereas smaller values of $\theta = 1.3$ and $\theta = 1.4$ are found in the neighbourhood (Figure S5, Supplement).

The production of $O_3$ is not solely instantaneous, but a gradual process. After the emission of both $NO_x$ and VOCs from point sources at and around the Landhuter Allee, air may be transported to the surroundings of the city of Munich, hence displacing both the already formed $O_3$ as well as the potential of the air to form $O_3$ *in situ*. This may be most pronounced when dilution during transport leads to lower $NO_x$ concentrations, as reductions in $NO_x$ can decrease $O_3$ titration and hence enhance $O_3$ concentrations in $NO_x$-limited regimes (Kirchner et al., 2001; Ren et al., 2022).

https://doi.org/10.5194/egusphere-2026-6529
Preprint. Discussion started: 2 November 2026
© Author(s) 2026. CC BY 4.0 License.

### 3.5 Temporal variability of the VOCs in the study area

In addition to the average spatial variability as presented and discussed in the above sections, we evaluated the temporal variability within each of the grid cells. In accordance with previous studies (Jobson et al., 1998; Karl et al., 2001; Williams et al., 2000), temporal variability was expressed as the standard deviation of the ln-transformed mixing ratios. This metric is unitless and reflects the spread in the data, with larger values indicating greater variability. Additionally, it is inversely proportional to the atmospheric lifetime across a set of compounds, given that there are no interfering factors. Here, this measure of variability was calculated for each VOC within each grid cell (limited to grid cells with more than 100 data points). The resulting VOC-specific variabilities were then averaged within each of the three VOC categories, namely the traffic-related VOCs (Figure 13a, n = 6), the biogenic VOCs (Figure 13b, n = 2), and the functionalized VOCs (Figure 13c, n = 4). The absolute value of the temporal variability, as well as the scope of the variability across the grid cells, is higher for the traffic-related VOCs (maximum 1.14, minimum at 48% of maximum) than for the biogenic VOCs (maximum 0.70, minimum at 76% of maximum) and the functionalized VOCs (maximum 0.42, minimum at 69% of maximum).

Generally, high variability can result from either high chemical reactivity or strong local source influence. On large spatial and temporal scales, variability is thought to be controlled by removal processes, making it a function of atmospheric lifetime. However, in cases where air is sampled in direct proximity to a substantial point source, this relationship can be disrupted, and the overall variability is likely to reflect source variability rather than reactive losses (Jobson et al., 1998; Karl et al., 2001; Williams et al., 2000). To test the degree to which the observed variability depends on either removal processes or nearby sources, we evaluated the relationship between the variability and the atmospheric lifetime for the group of traffic-related VOCs (n = 6) and for the joint group of biogenic and functionalized VOCs (n = 6). For each of these two groups, a linear regression was performed across all associated VOCs, with observations for every grid cell (Figure 14). To calculate the atmospheric lifetime of a given VOC, we considered only the reaction with OH radicals as the main daytime oxidative sink for most VOCs. Even for 2-methyl-2-pentene, which has the highest reactivity towards $O_3$, the pseudo first order loss rate against $O_3$ is still smaller than against OH radicals, assuming an average $O_3$ mixing ratio of 10 ppb in the Landshuter Allee area, and a OH radical concentration of $5\times10^6$ molecules $cm^{-3}$ which can be seen as a typical daytime OH radical concentration for this geographical region (Altshuller, 1989; Handisides et al., 2003). For the joint group of biogenic and functionalized VOCs, a negative relationship is observed between the mixing ratio variability and the lifetime against OH (slope = -0.08, $R^2$ = 0.68), demonstrating that a high reactivity is an important driver for the observed variability. For the traffic-related VOCs, on the other hand, there is only a weak dependence of the variability on the atmospheric lifetime (slope = -0.02, $R^2$ = 0.02), suggesting that the local source strength variability dominates the mixing ratio variability and impairs the variability-lifetime relationship.

https://doi.org/10.5194/egusphere-2026-6529
Preprint. Discussion started: 2 November 2026
© Author(s) 2026. CC BY 4.0 License.

This is important when considering that the traffic-related VOCs displayed the highest contributions to the ambient SOAP (Figure 12b) and OFP (Figure 12c) and are thus critical for local air pollution. Since the high mixing ratio variability of these compounds is largely driven by point sources, any reduction of these sources could have substantial benefits for air quality, especially considering the strongly VOC-limited $O_3$ production regime. This in turn creates scope for action on air quality measures and may be especially relevant for densely populated or frequented areas.

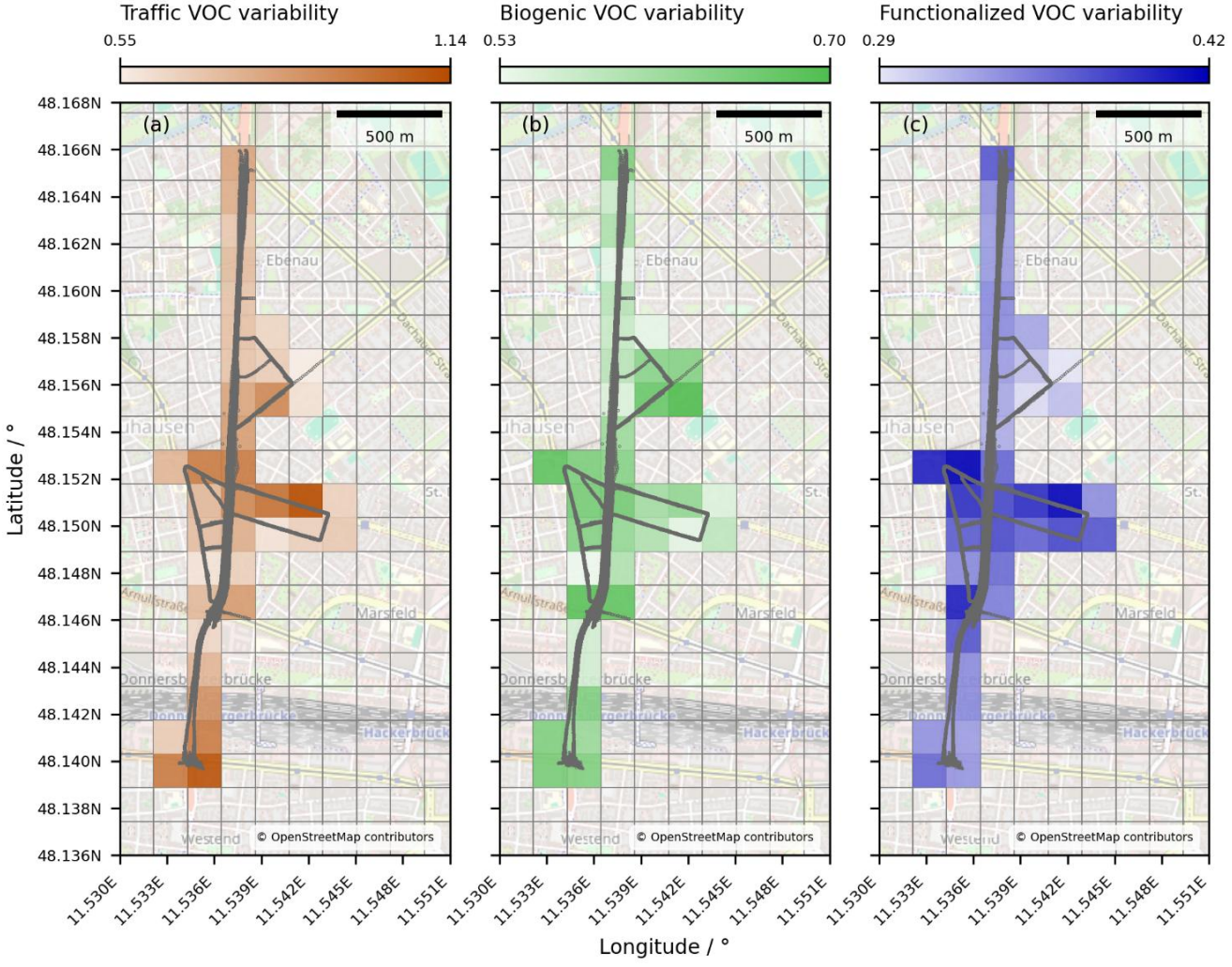



**Figure 13: Temporal variability of the VOC groups within each of the grid cells. Only grid cells with more than 100 data points were included. The variability was calculated for each individual VOC as the standard deviation of the logarithmic mixing ratios within the grid cell, and then averaged across all VOCs belonging to the VOC group. Base maps from OpenStreetMap, distributed under the Open Data Commons Open Database License (ODbL) v1.0, https://www.openstreetmap.org/copyright.**

https://doi.org/10.5194/egusphere-2026-6529
Preprint. Discussion started: 2 November 2026
© Author(s) 2026. CC BY 4.0 License.

675

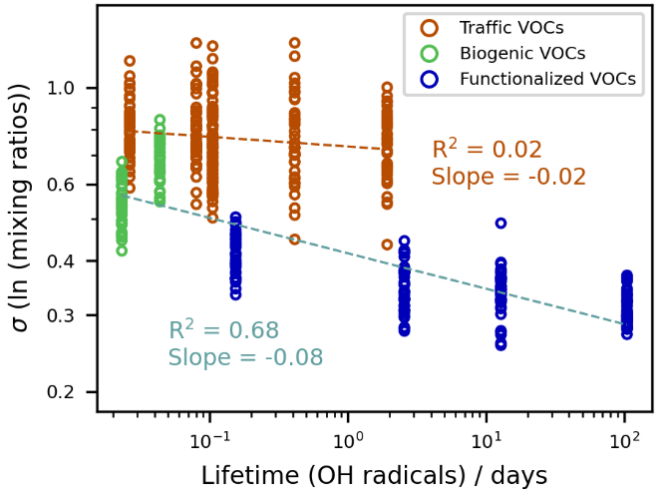



**Figure 14: Regression of the mixing ratio variability (determined as the standard deviation of the logarithmic values) against the lifetime in terms of the reaction with OH radicals (assuming [OH] = $5\times10^6$ molecules $cm^{-3}$], although the OH concentration only affects the x axis scale and not the overall pattern). Data are shown for each of the VOCs in the different VOC categories and for each of the grid cells with at least 100 data points. The data were fitted for traffic-related VOCs (n=6, slope -0.02, $R^2$ = 0.02), and**
680 **jointly for the biogenic and functionalized VOCs (n=6, slope -0.08, $R^2$ = 0.68).**

https://doi.org/10.5194/egusphere-2026-6529
Preprint. Discussion started: 2 November 2026
© Author(s) 2026. CC BY 4.0 License.

## 4 Conclusions

In this work, we used a mobile laboratory to measure mixing ratios of VOCs, $NO_x$, and $O_3$ in and around an urban street canyon with dense traffic in the city of Munich, Germany. Over the course of nine days, we collected data on different days of the week and at different times of the day as well as along different routes to characterize the overall spatio-temporal profile of the ambient air composition in the study area. The separation of the study area into grid cells allowed for a non-biased and objective statistical analysis. Based on their spatial similarities, three distinct VOC clusters were identified and interpreted as traffic-related compounds, biogenic compounds, and functionalized compounds respectively. The assessment of the contributions of removal processes and emissions to the temporal variability of the VOCs confirmed the importance of traffic as a local emission source and the allocation of the related compounds. In order to identify spatial differences, the grid cells were characterized and grouped through a combination of k-means clustering, hierarchical clustering, and NMDS. The results of these analyses were considered jointly to define focus areas that were investigated in more detail.

We found that the potential for air pollution differs substantially on spatial scales in the range of tens to hundreds of meters, although we acknowledge that higher differences may be found at even smaller scales e.g. in immediate proximity to vehicle exhaust systems. Across the different focus areas in the overall study area, the sum VOC mixing ratios didn't differ significantly, and the VOC pool was dominated by relatively slow-reacting oxygenated and functionalized VOCs. At the same time, considerable spatial differences were found with regard to oxidant loss rates and the potential for the formation of secondary pollutants. These differences can be ascribed to small-scale variations of some of the less abundant but more chemically active VOCs, such as VOCs emitted by traffic or vegetation. Although these did not account for a large part of the VOC sum, high reactivities and/or SOA and $O_3$ yields correspond to a substantial contribution to some of the photochemical parameters and therefore induce statistically significant spatial differences in urban air chemistry and quality. This is particularly true for traffic-related VOCs such as aromatics or alkenes, which displayed a high variability and also dominated the local potential for SOA and $O_3$ formation. The highest mixing ratios and impacts of these compounds were observed in the main street canyon in areas with dense infrastructure, whereas significantly lower potentials for pollution were identified for the street sections with less restricted airflows as well as for the neighbourhoods characterized by lighter traffic. These differences are particularly relevant for the cumulative exposure of residents and community members to airborne irritants and demonstrate the importance of not treating all locations within a bigger city as equal.

Thus, our results highlight the necessity and value of spatially resolved measurements of critical air constituents. Such approaches are essential for capturing the fine-scale variability of gases that is missed by monitoring networks with a limited number of stationary sites. This information is needed, in turn, for improving our understanding of air pollution and for identifying local exposure hotspots that are relevant for public health.

https://doi.org/10.5194/egusphere-2026-6529
Preprint. Discussion started: 2 November 2026
© Author(s) 2026. CC BY 4.0 License.

## Code and data availability

The code and data used in this study are available by request to the corresponding authors.

## Author contributions

IB, FL, JB, MF, and JS performed the mobile measurements. IB, LS, CKT, and ACN carried out preliminary work characterising the study area as a prerequisite for the measurement campaign presented in this study. FL was in charge of the formal analysis and visualization of the data. MS provided support for the statistical analyses. FL and ACN prepared the manuscript with contributions from all co-authors. ACN and CKT acquired funding and conceptualized the project.

## Competing interests

The authors declare that they have no conflict of interest.

## Acknowledgements

We would like to thank Andrej Einhorn for his support with managing the automated upload and back-up of the measurement data. We gratefully acknowledge the opportunity to park and charge the mobile laboratory at the Technical University of Munich (Technische Universität München) and the garden centre in Freising (Stadtgärtnerei Freising). We thank Regensburg University of Applied Sciences (Ostbayerische Technische Hochschule Regensburg) for lending us the nCLD instrument. This study was conducted as part of the REINELUFFT? project (reference number TLK01-L-76330, subproject AIR) funded by the Bavarian State Ministry of the Environment and Consumer Protection (Bayerisches Staatsministerium für Umwelt und Verbraucherschutz, StMUV). The article processing charges for this open-access publication were covered by the Forschungszentrum Jülich.

https://doi.org/10.5194/egusphere-2026-6529
Preprint. Discussion started: 2 November 2026
© Author(s) 2026. CC BY 4.0 License.

## References

de Abrantes, R., de Assunção, J. V., and Pesquero, C. R.: Emission of polycyclic aromatic hydrocarbons from light-duty diesel vehicles exhaust, Atmos. Environ., 38, 1631–1640, https://doi.org/10.1016/j.atmosenv.2003.11.012, 2004.

Altshuller, A. P.: Ambient Air Hydroxyl Radical Concentrations: Measurements and Model Predictions, JAPCA, 39, 704–708, https://doi.org/10.1080/08940630.1989.10466556, 1989.

Atkinson, R. W., Butland, B. K., Anderson, H. R., and Maynard, R. L.: Long-term Concentrations of Nitrogen Dioxide and Mortality: A Meta-analysis of Cohort Studies, Epidemiology, 29, 460, https://doi.org/10.1097/EDE.0000000000000847, 2018.

Bai, J., Guenther, A., Turnipseed, A., and Duhl, T.: Seasonal and interannual variations in whole-ecosystem isoprene and monoterpene emissions from a temperate mixed forest in Northern China, Atmos. Pollut. Res., 6, 696–707, https://doi.org/10.5094/APR.2015.078, 2015.

Baudic, A., Gros, V., Sauvage, S., Locoge, N., Sanchez, O., Sarda-Estève, R., Kalogridis, C., Petit, J.-E., Bonnaire, N., Baisnée, D., Favez, O., Albinet, A., Sciare, J., and Bonsang, B.: Seasonal variability and source apportionment of volatile organic compounds (VOCs) in the Paris megacity (France), Atmos. Chem. Phys., 16, 11961–11989, https://doi.org/10.5194/acp-16-11961-2016, 2016.

Beevers, S. D., Westmoreland, E., de Jong, M. C., Williams, M. L., and Carslaw, D. C.: Trends in $NO_x$ and $NO_2$ emissions from road traffic in Great Britain, Atmos. Environ., 54, 107–116, https://doi.org/10.1016/j.atmosenv.2012.02.028, 2012.

Coggon, M. M., McDonald, B. C., Vlasenko, A., Veres, P. R., Bernard, F., Koss, A. R., Yuan, B., Gilman, J. B., Peischl, J., Aikin, K. C., DuRant, J., Warneke, C., Li, S.-M., and de Gouw, J. A.: Diurnal Variability and Emission Pattern of Decamethylcyclopentasiloxane (D5) from the Application of Personal Care Products in Two North American Cities, Environ. Sci. Technol., 52, 5610–5618, https://doi.org/10.1021/acs.est.8b00506, 2018.

Coggon, M. M., Gkatzelis, G. I., McDonald, B. C., Gilman, J. B., Schwantes, R. H., Abuhassan, N., Aikin, K. C., Arend, M. F., Berkoff, T. A., Brown, S. S., Campos, T. L., Dickerson, R. R., Gronoff, G., Hurley, J. F., Isaacman-VanWertz, G., Koss, A. R., Li, M., McKeen, S. A., Moshary, F., Peischl, J., Pospisilova, V., Ren, X., Wilson, A., Wu, Y., Trainer, M., and Warneke, C.: Volatile chemical product emissions enhance ozone and modulate urban chemistry, Proc. Natl. Acad. Sci., 118, e2026653118, https://doi.org/10.1073/pnas.2026653118, 2021.

Coggon, M. M., Stockwell, C. E., Claflin, M. S., Pfannerstill, E. Y., Xu, L., Gilman, J. B., Marcantonio, J., Cao, C., Bates, K., Gkatzelis, G. I., Lamplugh, A., Katz, E. F., Arata, C., Apel, E. C., Hornbrook, R. S., Piel, F., Majluf, F., Blake, D. R., Wisthaler, A., Canagaratna, M., Lerner, B. M., Goldstein, A. H., Mak, J. E., and Warneke, C.: Identifying and correcting interferences to PTR-ToF-MS measurements of isoprene and other urban volatile organic compounds, Atmos. Meas. Tech., 17, 801–825, https://doi.org/10.5194/amt-17-801-2024, 2024.

Corrêa, S. M., Martins, E. M., and Arbilla, G.: Formaldehyde and acetaldehyde in a high traffic street of Rio de Janeiro, Brazil, Atmos. Environ., 37, 23–29, https://doi.org/10.1016/S1352-2310(02)00805-1, 2003.

Do, D. H., Van Langenhove, H., Chigbo, S. I., Amare, A. N., Demeestere, K., and Walgraeve, C.: Exposure to volatile organic compounds: Comparison among different transportation modes, Atmos. Environ., 94, 53–62, https://doi.org/10.1016/j.atmosenv.2014.05.019, 2014.

Duhl, T. R., Helmig, D., and Guenther, A.: Sesquiterpene emissions from vegetation: a review, Biogeosciences, 5, 761–777, https://doi.org/10.5194/bg-5-761-2008, 2008.

https://doi.org/10.5194/egusphere-2026-6529
Preprint. Discussion started: 2 November 2026
© Author(s) 2026. CC BY 4.0 License.

Dunmore, R. E., Whalley, L. K., Sherwen, T., Evans, M. J., Heard, D. E., Hopkins, J. R., Lee, J. D., Lewis, A. C., Lidster, R. T., Rickard, A. R., and Hamilton, J. F.: Atmospheric ethanol in London and the potential impacts of future fuel formulations, Faraday Discuss., 189, 105–120, https://doi.org/10.1039/C5FD00190K, 2016.

Geng, C. and Mu, Y.: Carbonyl sulfide and dimethyl sulfide exchange between trees and the atmosphere, Atmos. Environ., 40, 1373–1383, https://doi.org/10.1016/j.atmosenv.2005.10.023, 2006.

Gkatzelis, G. I., Coggon, M. M., McDonald, B. C., Peischl, J., Gilman, J. B., Aikin, K. C., Robinson, M. A., Canonaco, F., Prevot, A. S. H., Trainer, M., and Warneke, C.: Observations Confirm that Volatile Chemical Products Are a Major Source of Petrochemical Emissions in U.S. Cities, Environ. Sci. Technol., https://doi.org/10.1021/acs.est.0c05471, 2021.

de Gouw, J. A., Warneke, C., Parrish, D. D., Holloway, J. S., Trainer, M., and Fehsenfeld, F. C.: Emission sources and ocean uptake of acetonitrile ($CH_3CN$) in the atmosphere, J. Geophys. Res. Atmos., 108, https://doi.org/10.1029/2002JD002897, 2003.

Graus, M., Müller, M., and Hansel, A.: High Resolution PTR-TOF: Quantification and Formula Confirmation of VOC in Real Time, J. Am. Soc. Mass Spectrom., 21, 1037–1044, https://doi.org/10.1016/j.jasms.2010.02.006, 2010.

Guenther, A. B., Zimmerman, P. R., Harley, P. C., Monson, R. K., and Fall, R.: Isoprene and monoterpene emission rate variability: Model evaluations and sensitivity analyses, J. Geophys. Res. Atmos., 98, 12609–12617, https://doi.org/10.1029/93JD00527, 1993.

Guenther, A. B., Jiang, X., Heald, C. L., Sakulyanontvittaya, T., Duhl, T., Emmons, L. K., and Wang, X.: The Model of Emissions of Gases and Aerosols from Nature version 2.1 (MEGAN2.1): an extended and updated framework for modeling biogenic emissions, Geosci. Model Dev., 5, 1471–1492, https://doi.org/10.5194/gmd-5-1471-2012, 2012.

Gurjar, B. R., Jain, A., Sharma, A., Agarwal, A., Gupta, P., Nagpure, A. S., and Lelieveld, J.: Human health risks in megacities due to air pollution, Atmos. Environ., 44, 4606–4613, https://doi.org/10.1016/j.atmosenv.2010.08.011, 2010.

Haagen-Smit, A. J. and Fox, M. M.: Photochemical Ozone Formation with Hydrocarbons and Automobile Exhaust, Air Repair, 4, 105–136, https://doi.org/10.1080/00966665.1954.10467649, 1954.

Hallquist, M., Wenger, J. C., Baltensperger, U., Rudich, Y., Simpson, D., Claeys, M., Dommen, J., Donahue, N. M., George, C., Goldstein, A. H., Hamilton, J. F., Herrmann, H., Hoffmann, T., Iinuma, Y., Jang, M., Jenkin, M. E., Jimenez, J. L., Kiendler-Scharr, A., Maenhaut, W., McFiggans, G., Mentel, T. F., Monod, A., Prévôt, A. S. H., Seinfeld, J. H., Surratt, J. D., Szmigielski, R., and Wildt, J.: The formation, properties and impact of secondary organic aerosol: current and emerging issues, Atmos. Chem. Phys., 9, 5155–5236, https://doi.org/10.5194/acp-9-5155-2009, 2009.

Handisides, G. M., Plass-Dülmer, C., Gilge, S., Bingemer, H., and Berresheim, H.: Hohenpeissenberg Photochemical Experiment (HOPE 2000): Measurements and photostationary state calculations of OH and peroxy radicals, Atmos. Chem. Phys., 3, 1565–1588, https://doi.org/10.5194/acp-3-1565-2003, 2003.

Hantson, S., Knorr, W., Schurgers, G., Pugh, T. A. M., and Arneth, A.: Global isoprene and monoterpene emissions under changing climate, vegetation, $CO_2$ and land use, Atmos. Environ., 155, 35–45, https://doi.org/10.1016/j.atmosenv.2017.02.010, 2017.

Heikes, B. G., Chang, W., Pilson, M. E. Q., Swift, E., Singh, H. B., Guenther, A., Jacob, D. J., Field, B. D., Fall, R., Riemer, D., and Brand, L.: Atmospheric methanol budget and ocean implication, Glob. Biogeochem. Cycles, 16, 80-1-80–13, https://doi.org/10.1029/2002GB001895, 2002.

https://doi.org/10.5194/egusphere-2026-6529
Preprint. Discussion started: 2 November 2026
© Author(s) 2026. CC BY 4.0 License.

Henze, D. K., Seinfeld, J. H., Ng, N. L., Kroll, J. H., Fu, T.-M., Jacob, D. J., and Heald, C. L.: Global modeling of secondary organic aerosol formation from aromatic hydrocarbons: high- vs. low-yield pathways, Atmos. Chem. Phys., 8, 2405–2420, https://doi.org/10.5194/acp-8-2405-2008, 2008.

Hoek, G., Krishnan, R. M., Beelen, R., Peters, A., Ostro, B., Brunekreef, B., and Kaufman, J. D.: Long-term air pollution exposure and cardio- respiratory mortality: a review, Environ. Health, 12, 43, https://doi.org/10.1186/1476-069X-12-43, 2013.

Horowitz, L. W. and Jacob, D. J.: Global impact of fossil fuel combustion on atmospheric $NO_x$, J. Geophys. Res. Atmos., 104, 23823–23840, https://doi.org/10.1029/1999JD900205, 1999.

Isaacman-VanWertz, G., Frazier, G., Willison, J., and Faiola, C.: Missing Measurements of Sesquiterpene Ozonolysis Rates and Composition Limit Understanding of Atmospheric Reactivity, Environ. Sci. Technol., 58, 7937–7946, https://doi.org/10.1021/acs.est.3c10348, 2024.

Jacob, D. J., Field, B. D., Jin, E. M., Bey, I., Li, Q., Logan, J. A., Yantosca, R. M., and Singh, H. B.: Atmospheric budget of acetone, J. Geophys. Res. Atmos., 107, ACH 5-1-ACH 5-17, https://doi.org/10.1029/2001JD000694, 2002.

Jain, V., Tripathi, S. N., Tripathi, N., Sahu, L. K., Gaddamidi, S., Shukla, A. K., Bhattu, D., and Ganguly, D.: Seasonal variability and source apportionment of non-methane VOCs using PTR-TOF-MS measurements in Delhi, India, Atmos. Environ., 283, 119163, https://doi.org/10.1016/j.atmosenv.2022.119163, 2022.

Jensen, S. S., Larson, T., Deepti, K. C., and Kaufman, J. D.: Modeling traffic air pollution in street canyons in New York City for intra-urban exposure assessment in the US Multi-Ethnic Study of atherosclerosis and air pollution, Atmos. Environ., 43, 4544–4556, https://doi.org/10.1016/j.atmosenv.2009.06.042, 2009.

Jobson, B. T., Parrish, D. D., Goldan, P., Kuster, W., Fehsenfeld, F. C., Blake, D. R., Blake, N. J., and Niki, H.: Spatial and temporal variability of nonmethane hydrocarbon mixing ratios and their relation to photochemical lifetime, J. Geophys. Res. Atmos., 103, 13557–13567, https://doi.org/10.1029/97JD01715, 1998.

Jordan, A., Hansel, A., Holzinger, R., and Lindinger, W.: Acetonitrile and benzene in the breath of smokers and non-smokers investigated by proton transfer reaction mass spectrometry (PTR-MS), Int. J. Mass Spectrom. Ion Process., 148, L1–L3, https://doi.org/10.1016/0168-1176(95)04236-E, 1995.

Kang, S., Kim, J.-A., Lee, M., Park, J., Jeon, E., Shim, M., and Shin, Y.: An analysis of the temporal variability in volatile organic compounds (VOCs) within megacity Seoul and an identification of their sources, Atmos. Pollut. Res., 13, 101338, https://doi.org/10.1016/j.apr.2022.101338, 2022.

Karl, T., Crutzen, P. J., Mandl, M., Staudinger, M., Guenther, A., Jordan, A., Fall, R., and Lindinger, W.: Variability-lifetime relationship of VOCs observed at the Sonnblick Observatory 1999—estimation of HO-densities, Atmos. Environ., 35, 5287–5300, https://doi.org/10.1016/S1352-2310(01)00341-7, 2001.

Karl, T., Striednig, M., Graus, M., Hammerle, A., and Wohlfahrt, G.: Urban flux measurements reveal a large pool of oxygenated volatile organic compound emissions, Proc. Natl. Acad. Sci., 115, 1186–1191, https://doi.org/10.1073/pnas.1714715115, 2018.

Keuken, M., Roemer, M., and van den Elshout, S.: Trend analysis of urban $NO_2$ concentrations and the importance of direct $NO_2$ emissions versus ozone/$NO_x$ equilibrium, Atmos. Environ., 43, 4780–4783, https://doi.org/10.1016/j.atmosenv.2008.07.043, 2009.

https://doi.org/10.5194/egusphere-2026-6529
Preprint. Discussion started: 2 November 2026
© Author(s) 2026. CC BY 4.0 License.

Kirchner, F., Jeanneret, F., Clappier, A., Krüger, B., van den Bergh, H., and Calpini, B.: Total VOC reactivity in the planetary boundary layer: 2. A new indicator for determining the sensitivity of the ozone production to VOC and $NO_x$, J. Geophys. Res. Atmos., 106, 3095–3110, https://doi.org/10.1029/2000JD900603, 2001.

Koss, A., Yuan, B., Warneke, C., Gilman, J. B., Lerner, B. M., Veres, P. R., Peischl, J., Eilerman, S., Wild, R., Brown, S. S., Thompson, C. R., Ryerson, T., Hanisco, T., Wolfe, G. M., Clair, J. M. S., Thayer, M., Keutsch, F. N., Murphy, S., and de Gouw, J.: Observations of VOC emissions and photochemical products over US oil- and gas-producing regions using high-resolution $H_3O^+$ CIMS (PTR-ToF-MS), Atmos. Meas. Tech., 10, 2941–2968, https://doi.org/10.5194/amt-10-2941-2017, 2017.

Kreft, H. and Jetz, W.: A framework for delineating biogeographical regions based on species distributions, J. Biogeogr., 37, 2029–2053, https://doi.org/10.1111/j.1365-2699.2010.02375.x, 2010.

Kumar, A., O'Leary, C., Winkless, R., Thompson, M., L. Davies, H., Shaw, M., J. Andrews, S., Carslaw, N., and J. Dillon, T.: Fingerprinting the emissions of volatile organic compounds emitted from the cooking of oils, herbs, and spices, Environ. Sci. Process. Impacts, 27, 244–261, https://doi.org/10.1039/D4EM00579A, 2025.

Lal, S., Naja, M., and Subbaraya, B. H.: Seasonal variations in surface ozone and its precursors over an urban site in India, Atmos. Environ., 34, 2713–2724, https://doi.org/10.1016/S1352-2310(99)00510-5, 2000.

Legendre, P. and Legendre, L.: Numerical Ecology - Second Edition, Elsevier, Amsterdam, ISBN 978-0-444-89249-2, 1998.

Lelieveld, J., Butler, T. M., Crowley, J. N., Dillon, T. J., Fischer, H., Ganzeveld, L., Harder, H., Lawrence, M. G., Martinez, M., Taraborrelli, D., and Williams, J.: Atmospheric oxidation capacity sustained by a tropical forest, Nature, 452, 737–740, https://doi.org/10.1038/nature06870, 2008.

Lewis, A. C.: The changing face of urban air pollution, Science, 359, 744–745, https://doi.org/10.1126/science.aar4925, 2018.

Li, X.-B., Yuan, B., Wang, S., Wang, C., Lan, J., Liu, Z., Song, Y., He, X., Huangfu, Y., Pei, C., Cheng, P., Yang, S., Qi, J., Wu, C., Huang, S., You, Y., Chang, M., Zheng, H., Yang, W., Wang, X., and Shao, M.: Variations and sources of volatile organic compounds (VOCs) in urban region: insights from measurements on a tall tower, Atmos. Chem. Phys., 22, 10567–10587, https://doi.org/10.5194/acp-22-10567-2022, 2022.

Li, X.-B., Yuan, B., Huangfu, Y., Yang, S., Song, X., Qi, J., He, X., Wang, S., Chen, Y., Yang, Q., Song, Y., Peng, Y., Tang, G., Gao, J., Gu, D., and Shao, M.: Vertical changes in volatile organic compounds (VOCs) and impacts on photochemical ozone formation, Atmos. Chem. Phys., 25, 2459–2472, https://doi.org/10.5194/acp-25-2459-2025, 2025.

Liang, Q., Bao, X., Sun, Q., Zhang, Q., Zou, X., Huang, C., Shen, C., and Chu, Y.: Imaging VOC distribution in cities and tracing VOC emission sources with a novel mobile proton transfer reaction mass spectrometer, Environ. Pollut., 265, 114628, https://doi.org/10.1016/j.envpol.2020.114628, 2020.

Lindinger, W., Hansel, A., and Jordan, A.: On-line monitoring of volatile organic compounds at pptv levels by means of proton-transfer-reaction mass spectrometry (PTR-MS) medical applications, food control and environmental research, Int. J. Mass Spectrom. Ion Process., 173, 191–241, https://doi.org/10.1016/S0168-1176(97)00281-4, 1998.

Martens, P., Czech, H., Tissari, J., Ihalainen, M., Suhonen, H., Sklorz, M., Jokiniemi, J., Sippula, O., and Zimmermann, R.: Emissions of Gases and Volatile Organic Compounds from Residential Heating: A Comparison of Brown Coal Briquettes and Logwood Combustion, Energy Fuels, 35, 14010–14022, https://doi.org/10.1021/acs.energyfuels.1c01667, 2021.

https://doi.org/10.5194/egusphere-2026-6529
Preprint. Discussion started: 2 November 2026
© Author(s) 2026. CC BY 4.0 License.

Masiol, M., Squizzato, S., Rich, D. Q., and Hopke, P. K.: Long-term trends (2005–2016) of source apportioned PM2.5 across New York State, Atmos. Environ., 201, 110–120, https://doi.org/10.1016/j.atmosenv.2018.12.038, 2019.

McDonald, B. C., de Gouw, J. A., Gilman, J. B., Jathar, S. H., Akherati, A., Cappa, C. D., Jimenez, J. L., Lee-Taylor, J., Hayes, P. L., McKeen, S. A., Cui, Y. Y., Kim, S.-W., Gentner, D. R., Isaacman-VanWertz, G., Goldstein, A. H., Harley, R. A., Frost, G. J., Roberts, J. M., Ryerson, T. B., and Trainer, M.: Volatile chemical products emerging as largest petrochemical source of urban organic emissions, Science, 359, 760–764, https://doi.org/10.1126/science.aaq0524, 2018.

Mellouki, A., Wallington, T. J., and Chen, J.: Atmospheric Chemistry of Oxygenated Volatile Organic Compounds: Impacts on Air Quality and Climate, Chem. Rev., 115, 3984–4014, https://doi.org/10.1021/cr500549n, 2015.

Millet, D. B., Guenther, A., Siegel, D. A., Nelson, N. B., Singh, H. B., de Gouw, J. A., Warneke, C., Williams, J., Eerdekens, G., Sinha, V., Karl, T., Flocke, F., Apel, E., Riemer, D. D., Palmer, P. I., and Barkley, M.: Global atmospheric budget of acetaldehyde: 3-D model analysis and constraints from in-situ and satellite observations, Atmos. Chem. Phys., 10, 3405–3425, https://doi.org/10.5194/acp-10-3405-2010, 2010.

Ng, N. L., Chhabra, P. S., Chan, A. W. H., Surratt, J. D., Kroll, J. H., Kwan, A. J., McCabe, D. C., Wennberg, P. O., Sorooshian, A., Murphy, S. M., Dalleska, N. F., Flagan, R. C., and Seinfeld, J. H.: Effect of $NO_x$ level on secondary organic aerosol (SOA) formation from the photooxidation of terpenes, Atmos. Chem. Phys., 7, 5159–5174, https://doi.org/10.5194/acp-7-5159-2007, 2007.

Pfannerstill, E. Y., Arata, C., Zhu, Q., Schulze, B. C., Woods, R., Harkins, C., Schwantes, R. H., McDonald, B. C., Seinfeld, J. H., Bucholtz, A., Cohen, R. C., and Goldstein, A. H.: Comparison between Spatially Resolved Airborne Flux Measurements and Emission Inventories of Volatile Organic Compounds in Los Angeles, Environ. Sci. Technol., 57, 15533–15545, https://doi.org/10.1021/acs.est.3c03162, 2023.

Pfannerstill, E. Y., Arata, C., Zhu, Q., Schulze, B. C., Ward, R., Woods, R., Harkins, C., Schwantes, R. H., Seinfeld, J. H., Bucholtz, A., Cohen, R. C., and Goldstein, A. H.: Temperature-dependent emissions dominate aerosol and ozone formation in Los Angeles, Science, 384, 1324–1329, https://doi.org/10.1126/science.adg8204, 2024.

Prinn, R. G.: The Cleansing Capacity of the Atmosphere, Annu. Rev. Environ. Resour., 28, 29–57, https://doi.org/10.1146/annurev.energy.28.011503.163425, 2003.

Ren, J., Guo, F., and Xie, S.: Diagnosing ozone–$NO_x$–VOC sensitivity and revealing causes of ozone increases in China based on 2013–2021 satellite retrievals, Atmos. Chem. Phys., 22, 15035–15047, https://doi.org/10.5194/acp-22-15035-2022, 2022.

Romano, A. and Hanna, G. B.: Identification and quantification of VOCs by proton transfer reaction time of flight mass spectrometry: An experimental workflow for the optimization of specificity, sensitivity, and accuracy, J. Mass Spectrom., 53, 287–295, https://doi.org/10.1002/jms.4063, 2018.

Rutherford, M., Koss, A., and de Gouw, J.: Mobile VOC measurements in Commerce City, CO reveal the emissions from different sources, J. Air Waste Manag. Assoc., 74, 714–725, https://doi.org/10.1080/10962247.2024.2379927, 2024.

Schmitz, T., Hassel, D., and Weber, F.-J.: Determination of VOC-components in the exhaust of gasoline and diesel passenger cars, Atmos. Environ., 34, 4639–4647, https://doi.org/10.1016/S1352-2310(00)00303-4, 2000.

Sheng, J., Zhao, D., Ding, D., Li, X., Huang, M., Gao, Y., Quan, J., and Zhang, Q.: Characterizing the level, photochemical reactivity, emission, and source contribution of the volatile organic compounds based on PTR-TOF-MS during winter haze period in Beijing, China, Atmos. Res., 212, 54–63, https://doi.org/10.1016/j.atmosres.2018.05.005, 2018.

https://doi.org/10.5194/egusphere-2026-6529
Preprint. Discussion started: 2 November 2026
© Author(s) 2026. CC BY 4.0 License.

Shi, Z., Salim Alam, M., and Nikolova, I.: Highlights from Faraday Discussion: Chemistry in the urban atmosphere, United Kingdom, April 2016, Chem. Commun., 52, 9162–9172, https://doi.org/10.1039/C6CC90296K, 2016.

Sungur, L., Bamberger, I., Schneider, J., Bachmann, F., Nölscher, A. C., and Thomas, C. K.: The impact of synoptic forcing and vehicle traffic on atmospheric transport processes and $NO_2$ concentrations in a highly polluted urban street canyon, Atmos. Pollut. Res., 102965, https://doi.org/10.1016/j.apr.2026.102965, 2026.

Sweet, C. W. and Vermette, S. J.: Toxic volatile organic compounds in urban air in Illinois, Environ. Sci. Technol., 26, 165–173, https://doi.org/10.1021/es00025a020, 1992.

Tani, A., Hayward, S., and Hewitt, C. N.: Measurement of monoterpenes and related compounds by proton transfer reaction-mass spectrometry (PTR-MS), Int. J. Mass Spectrom., 223–224, 561–578, https://doi.org/10.1016/S1387-3806(02)00880-1, 2003.

Valach, A. C., Langford, B., Nemitz, E., MacKenzie, A. R., and Hewitt, C. N.: Seasonal and diurnal trends in concentrations and fluxes of volatile organic compounds in central London, Atmos. Chem. Phys., 15, 7777–7796, https://doi.org/10.5194/acp-15-7777-2015, 2015.

in 't Veld, M., Seco, R., Reche, C., Pérez, N., Alastuey, A., Portillo-Estrada, M., Janssens, I. A., Peñuelas, J., Fernandez-Martinez, M., Marchand, N., Temime-Roussel, B., Querol, X., and Yáñez-Serrano, A. M.: Identification of volatile organic compounds and their sources driving ozone and secondary organic aerosol formation in NE Spain, Sci. Total Environ., 906, 167159, https://doi.org/10.1016/j.scitotenv.2023.167159, 2024.

Wagner, R. L., Farren, N. J., Davison, J., Young, S., Hopkins, J. R., Lewis, A. C., Carslaw, D. C., and Shaw, M. D.: Application of a mobile laboratory using a selected-ion flow-tube mass spectrometer (SIFT-MS) for characterisation of volatile organic compounds and atmospheric trace gases, Atmos. Meas. Tech., 14, 6083–6100, https://doi.org/10.5194/amt-14-6083-2021, 2021.

Wang, A., Fallah-Shorshani, M., Xu, J., and Hatzopoulou, M.: Characterizing near-road air pollution using local-scale emission and dispersion models and validation against in-situ measurements, Atmos. Environ., 142, 452–464, https://doi.org/10.1016/j.atmosenv.2016.08.020, 2016a.

Wang, G., Cheng, S., Lang, J., Li, S., and Tian, L.: On-board measurements of gaseous pollutant emission characteristics under real driving conditions from light-duty diesel vehicles in Chinese cities, J. Environ. Sci., 46, 28–37, https://doi.org/10.1016/j.jes.2015.09.021, 2016b.

Wang, N., Ernle, L., Bekö, G., Wargocki, P., and Williams, J.: Emission Rates of Volatile Organic Compounds from Humans, Environ. Sci. Technol., 56, 4838–4848, https://doi.org/10.1021/acs.est.1c08764, 2022.

Wang, W., Yan, Y., Fang, H., Li, J., Zha, S., and Wu, T.: Volatile organic compound emissions from typical industries: Implications for the importance of oxygenated volatile organic compounds, Atmos. Pollut. Res., 14, 101640, https://doi.org/10.1016/j.apr.2022.101640, 2023.

Wilde, S. E., Padilla, L. E., Farren, N. J., Alvarez, R. A., Wilson, S., Lee, J. D., Wagner, R. L., Slater, G., Peters, D., and Carslaw, D. C.: Mobile monitoring reveals congestion penalty for vehicle emissions in London, Atmos. Environ. X, 21, 100241, https://doi.org/10.1016/j.aeaoa.2024.100241, 2024.

Williams, J., Fischer, H., Harris, G. W., Crutzen, P. J., Hoor, P., Hansel, A., Holzinger, R., Warneke, C., Lindinger, W., Scheeren, B., and Lelieveld, J.: Variability-lifetime relationship for organic trace gases: A novel aid to compound identification

https://doi.org/10.5194/egusphere-2026-6529
Preprint. Discussion started: 2 November 2026
© Author(s) 2026. CC BY 4.0 License.



and estimation of HO concentrations, J. Geophys. Res. Atmos., 105, 20473–20486, https://doi.org/10.1029/2000JD900203, 2000.

Wilson, S., Farren, N. J., Wilde, S. E., Wagner, R. L., Lee, J. D., Padilla, L. E., Slater, G., Peters, D., and Carslaw, D. C.: Mobile monitoring reveals the importance of non-vehicular particulate matter sources in London, Environ. Sci. Process. Impacts, 26, 2145–2157, https://doi.org/10.1039/D4EM00552J, 2024.

Wu, C., Wang, C., Wang, S., Wang, W., Yuan, B., Qi, J., Wang, B., Wang, H., Wang, C., Song, W., Wang, X., Hu, W., Lou, S., Ye, C., Peng, Y., Wang, Z., Huangfu, Y., Xie, Y., Zhu, M., Zheng, J., Wang, X., Jiang, B., Zhang, Z., and Shao, M.: Measurement report: Important contributions of oxygenated compounds to emissions and chemistry of volatile organic compounds in urban air, Atmos. Chem. Phys., 20, 14769–14785, https://doi.org/10.5194/acp-20-14769-2020, 2020.

Yuan, B., Shao, M., de Gouw, J., Parrish, D. D., Lu, S., Wang, M., Zeng, L., Zhang, Q., Song, Y., Zhang, J., and Hu, M.: Volatile organic compounds (VOCs) in urban air: How chemistry affects the interpretation of positive matrix factorization (PMF) analysis, J. Geophys. Res. Atmos., 117, https://doi.org/10.1029/2012JD018236, 2012.

Zhang, H., Li, H., Zhang, Q., Zhang, Y., Zhang, W., Wang, X., Bi, F., Chai, F., Gao, J., Meng, L., Yang, T., Chen, Y., Cheng, Q., and Xia, F.: Atmospheric Volatile Organic Compounds in a Typical Urban Area of Beijing: Pollution Characterization, Health Risk Assessment and Source Apportionment, Atmosphere, 8, 61, https://doi.org/10.3390/atmos8030061, 2017.

Zhao, Y., Li, Y., Kumar, A., Ying, Q., Vandenberghe, F., and Kleeman, M. J.: Separately resolving $NO_x$ and VOC contributions to ozone formation, Atmos. Environ., 285, 119224, https://doi.org/10.1016/j.atmosenv.2022.119224, 2022.

Zhu, Y., Chen, J., Bi, X., Kuhlmann, G., Chan, K. L., Dietrich, F., Brunner, D., Ye, S., and Wenig, M.: Spatial and temporal representativeness of point measurements for nitrogen dioxide pollution levels in cities, Atmos. Chem. Phys., 20, 13241–13251, https://doi.org/10.5194/acp-20-13241-2020, 2020.